Rigorous Derivation and Fast Solution of Spatial-Domain Green's Functions for Uniaxial Anisotropic Multilayers Using Modified Fast Hankel Transform Method

Ping-Ping Ding, Cheng-Wei Qiu, *Member, IEEE*, Saïd Zouhdi, *Senior Member, IEEE*, and Swee Ping Yeo

***Abstract*—A fast solution for rigorously deriving and calculating spatial-domain dyadic Green's functions for the planar multilayers of uniaxial media has been established based on the modified fast Hankel transform (MFHT) method. The *kDB* coordinate system is exploited and integrated with the wave iterative technique to obtain the spectral-domain Green's function. This algorithm relies on the accurate expressions of unbounded dyadic Green's function and scattered Green's function in uniaxial media, which can be classified into the ordinary and extraordinary waves. The newly developed MFHT method is then employed for the calculation of the dyadic Green's function in the planar multilayered uniaxial anisotropic media. The validity of the algorithm thus developed and the efficiency of the MFHT method are verified through numerical examples. The spatial-domain Green's function can, for the first time, deal with the multilayered uniaxial anisotropic media, and more importantly, the influence of material's anisotropy upon the Green's function is demonstrated. It provides a promising tool to analyze the integrated microwave circuits and optical devices when complex materials are involved.**

***Index Terms*—Dyadic Green's function, *kDB* coordinate system, modified fast Hankel transform (MFHT) method, multilayered structure, spatial domain, uniaxial anisotropic media.**

I. Introduction

INTEGRAL equation methods have been a versatile and valuable tool for the electromagnetic analysis of microwave integrated circuits and microstrip antennas implemented in planar multilayered substrates [1]–[4]. The electric and magnetic fields in the multilayered structures can be easily derived from the dyadic Green's function and the computational efficiency is strongly dependent on the calculation of the dyadic Green's function. Consequently, a large amount of research has been dedicated to the calculation of the dyadic Green's functions in the multilayered isotropic media over the last decades [5]–[13]. Due to the emergence of practical applications of complex media in multilayered geometries [14]–[17], the accurate and expedient calculation of the multilayered Green's function in both the spectral and spatial domains is highly necessary and important as a characterization tool. Several effective methods [18]–[20] have been proposed for the derivation of the spectral-domain Green's function in the multilayered uniaxial anisotropic media, e.g., the cylindrical vector eigenfunction expansion technique [21] and wave iterative technique [22], [23]. A brief review of the two methods is given below.

The main idea of the cylindrical vector eigenfunction expansion technique is to expand the unbounded Green's function in terms of the solenoidal and irrotational cylindrical vector wave functions according to the Ohm–Rayleigh method [24], [25] and the scattered dyadic Green's function is thereafter derived by applying the principle of scattering superposition. The cylindrical vector eigenfunction expansion technique is straightforward. However, the coefficients of the scattered dyadic Green's function cannot be analytically expressed by explicit formulations for an arbitrary number of planar layers. Although the calculation of scattering coefficients is still possible when the medium is composed of one or two layers, it becomes a cumbersome step for the case of multilayered media. Therefore, it is difficult, if not impossible, to employ the cylindrical vector eigenfunction expansion technique for the systematic derivation of dyadic Green's function for multilayered uniaxial anisotropic media.

The wave iterative technique employs the *kDB* coordinate system to obtain the characteristic field vectors and the Fourier transform to derive the unbounded Green's function. Subsequently, based on the boundary condition and wave iterative technique, the scattered Green's function in the spectral domain is derived. The spectral-domain Green's functions are expressed in terms of ordinary and extraordinary waves and the derivation process is straightforward and flexible. However, there is one primary problem for the derivation of the spectral-domain Green's function in [23]. In the derivation of the Green's function in the total field, the vertical position of one interface related with the source layer has to be set to zero. This implies that, whenever the source position is changed, the whole coordinate system should be reset, which, in turn, will introduce particular complexity in the implementation of the numerical computation. Therefore, the theoretical formulas in [23] are not

Manuscript received April 29, 2011; revised October 13, 2011; accepted October 21, 2011. Date of publication December 08, 2011; date of current version February 03, 2012. This work was supported by the National University of Singapore under Grant R-263-000-663-646 and Grant R-263-000-663-232.

P.-P. Ding, C.-W. Qiu, and S. P. Yeo are with the Department of Electrical and Computer Engineering, National University of Singapore, Singapore 117583 (e-mail: g0700206@nus.edu.sg; chengwei.qiu@nus.edu.sg; eleyeosp@nus.edu.sg).

S. Zouhdi is with the Laboratoire de Génie Electrique de Paris, SUPELEC, 91192 Gif-sur-Yvette, France (e-mail: said.zouhdi@supelec.fr).

Color versions of one or more of the figures in this paper are available online at http://ieeexplore.ieee.org.

Digital Object Identifier 10.1109/TMTT.2011.2175941

able to efficiently treat general multilayered problems with arbitrary positions of the source.

The fast Hankel transform (FHT) method was employed as a fast solution to the computation of Green's functions for isotropic multilayers [26]. The main idea of the FHT method is to transform the Sommerfeld integral into a linear discrete convolution and the convolution results can be regarded as the system response of a digital filter. However, based on the FHT filter technique, it can be difficult to obtain accurate dyadic Green's function because of the branch-cut singularity and the surface wave poles singularity. Although the singularities can be completely avoided through deforming the integration path of the Hankel transform from the real axis, the argument of the integral kernel becomes a complex number, and thus the FHT algorithm is not directly applicable. The modified fast Hankel transform (MFHT) algorithm [27] has been proposed to overcome this problem by deforming the integration path from the real axis to the quadrant so as to avoid the singularities. Subsequently the Bessel function with a complex argument can be expressed as a sum of products of two Bessel functions, respectively, with the real part and imaginary part of the original complex argument. The FHT filter technique can then be applied to each expansion term.

The MFHT method successfully extends the applicability of the conventional FHT method to general multilayered geometries and it is an attractive alternative to the rigorous, but computationally expensive numerical integration method. Compared with the well-known two-level discrete complex image method (DCIM), the MFHT method also shows superior efficiency when the vertical position of the source point or observation point needs to be changed frequently. Based on the newly developed MFHT method, the fast solutions of dyadic Green's functions used in the electric/magnetic field integral equation are, for the first time, obtained for the planar multilayered uniaxial anisotropic media. The robustness of the algorithm thus developed and the accuracy and efficiency of the dyadic Green's function will be validated. Finally, the influence of material anisotropy on the dyadic Green's function will be illustrated.

II. Unbounded Dyadic Green's Function for a Uniaxial Anisotropic Medium

In this section, we will derive the dyadic Green's function for an unbounded uniaxial anisotropic medium. By using the kDB coordinate system and the Fourier transform method, the electric field Green's function will be derived, and then the electric and magnetic fields can be obtained for an arbitrarily distributed electric current source. The fields are assumed to be time–harmonic, and for convenience, the associated factor $e^{-i\omega t}$ will not be expressly included in this paper. A uniaxial anisotropic medium is characterized by scalar magnetic permeability μ and electric permittivity tensor $\overline{\overline{\varepsilon}}$. When the optic axis of the uniaxial anisotropic medium is in the $\hat{z}$-direction, the permittivity tensor is

$$\overline{\overline{\varepsilon}} = \begin{bmatrix} \varepsilon_t & 0 & 0 \\ 0 & \varepsilon_t & 0 \\ 0 & 0 & \varepsilon_z \end{bmatrix}. \tag{1}$$

In the xyz coordinate system, the constitutive relations in the uniaxial anisotropic medium are

$$\mathbf{E} = \overline{\overline{\kappa}} \cdot \mathbf{D} \tag{2}$$
$$\mathbf{H} = \nu \mathbf{B} \tag{3}$$

where

$$\overline{\overline{\kappa}} = \overline{\overline{\varepsilon}}^{-1} = \begin{bmatrix} \kappa & 0 & 0 \\ 0 & \kappa & 0 \\ 0 & 0 & \kappa_z \end{bmatrix} \tag{4}$$
$$\nu = \mu^{-1} \tag{5}$$

$\overline{\overline{\kappa}}$ is the impermittivity tensor. It is known that there are two distinct characteristic waves, ordinary wave and extraordinary wave, for the uniaxial anisotropic medium [28]. Their dispersion relations are

$$\omega^2 = \nu\kappa k_z^2 + \nu\kappa k_s^2 \tag{6}$$

for the ordinary wave and

$$\omega^2 = \nu\kappa k_z^2 + \nu\kappa_z k_s^2 \tag{7}$$

for the extraordinary wave. The solutions to (6) and (7) include the roots $k_z = \pm k_{zo}$ and $k_z = \pm k_{ze}$, respectively. The subscripts o and e denote the ordinary wave and extraordinary wave, respectively, and the subscripts u and d refer to the upward propagating wave and downward propagating wave, respectively. By using the kDB system, the electric and magnetic fields in the xyz coordinate system can be represented as

$$\mathbf{E}(\mathbf{k}) = \overline{\overline{\kappa}} \cdot [D_1(\mathbf{k})\hat{h} - D_2(\mathbf{k})\hat{v}(k_z)] \tag{8}$$
$$\mathbf{H}(\mathbf{k}) = -\frac{\omega}{k}[D_2(\mathbf{k})\hat{h} + D_1(\mathbf{k})\hat{v}(k_z)] \tag{9}$$

where

$$\hat{h} = \frac{1}{k_s}(\hat{x}\,k_y - \hat{y}\,k_x) \tag{10}$$
$$\hat{v} = \frac{1}{k}(-k_z\,\hat{k}_s + k_s\,\hat{z}) \tag{11}$$
$$\hat{k}_s = \frac{1}{k_s}(\hat{x}\,k_x + \hat{y}\,k_y) \tag{12}$$

$D_{1,2}$ represents the two components of $\mathbf{D}$ projected onto the kDB coordinator system. Considering the roots of the dispersion relations (6) and (7), we can write the characteristic field vectors as follows:

$$\begin{aligned} \mathbf{e}_{\alpha\beta}(\mathbf{k}_s) &\equiv \mathbf{E}(\mathbf{k}_s, \pm k_{z\alpha}) \\ &= \overline{\overline{\kappa}} \cdot [D_{1\alpha}(\mathbf{k})\hat{h} - D_{2\alpha}(\mathbf{k})\hat{v}(\pm k_{z\alpha})] \end{aligned} \tag{13}$$
$$\begin{aligned} \mathbf{h}_{\alpha\beta}(\mathbf{k}_s) &\equiv \mathbf{H}(\mathbf{k}_s, \pm k_{z\alpha}) \\ &= -\frac{\omega}{k_\alpha}[D_{2\alpha}(\mathbf{k})\hat{h} + D_{1\alpha}(\mathbf{k})\hat{v}(\pm k_{z\alpha})] \end{aligned} \tag{14}$$

where

$$k_\alpha^2 = k_s^2 + k_{z\alpha}^2 \tag{15}$$

and $\alpha = o, e$; $\beta = u, d$. In the Fourier spectral domain, the electric field $\mathbf{E}(\mathbf{k}_s; z \backslash z')$ $(z \neq z')$ can be expressed as a superposition of ordinary and extraordinary waves

$$\begin{aligned}\mathbf{E}(\mathbf{k}_s; z\backslash z') &= \frac{1}{(2\pi)^2}\int_{-\infty}^{\infty} e^{-i\mathbf{k}_s\cdot(\mathbf{r}_s-\mathbf{r}_s')}\mathbf{E}(\mathbf{r},\mathbf{r}')d\mathbf{r}_s \\ &= A_{o\beta}(\mathbf{k}_s)\mathbf{e}_{o\beta}(\mathbf{k}_s)e^{\pm ik_{zo}(z-z')} \\ &\quad + A_{e\beta}(\mathbf{k}_s)\mathbf{e}_{e\beta}(\mathbf{k}_s)e^{\pm ik_{ze}(z-z')}. \qquad (16)\end{aligned}$$

The primed and unprimed parameters correspond to the source and observation points, respectively. In this study, we assume that the electric current point source is arbitrarily oriented, which is expressed by

$$\mathbf{J}(\mathbf{r}) = \hat{a}\delta(\mathbf{r}-\mathbf{r}') \qquad (17)$$

where $\hat{a}$ is an arbitrary unit vector. In order to obtain the unknown values of amplitudes $A_{\alpha\beta}(\mathbf{k}_s)$, we employ the spectral-domain wave equation to formulate the electric field

$$\mathbf{L}(\mathbf{k})\cdot\mathbf{E}(\mathbf{k}) = i\omega\mu\mathbf{J}(\mathbf{k}_s, k_z) \qquad (18)$$

where

$$\mathbf{J}(\mathbf{k}_s, k_z) = \frac{1}{(2\pi)^3}\hat{a} \qquad (19)$$

$\mathbf{L}(\mathbf{k})$ is the dyadic Helmholtz operator for the uniaxial anisotropic medium

$$\mathbf{L}(\mathbf{k}) = k^2\mathbf{I} - \omega^2\mu\bar{\bar{\varepsilon}} - \mathbf{kk}. \qquad (20)$$

After algebraic manipulations, (20) can be recast in the following form:

$$\begin{aligned}\mathbf{L}(\mathbf{k}) &= k_\alpha^2\mathbf{I} - \omega^2\mu\bar{\bar{\varepsilon}} - \mathbf{k}_{\alpha\beta}\mathbf{k}_{\alpha\beta} \\ &\quad + (k_z^2 - k_{z\alpha}^2)(\hat{h}\hat{h} + \hat{k}_s\hat{k}_s) \\ &\quad - k_s[k_z - (\pm k_{z\alpha})](\hat{z}\hat{k}_s + \hat{k}_s\hat{z}). \qquad (21)\end{aligned}$$

By using the Fourier transform and (16), the expression of $\mathbf{E}(\mathbf{k})$ can be written as [23]

$$\begin{aligned}\mathbf{E}(\mathbf{k}) &= \frac{1}{2\pi}\int_{-\infty}^{\infty} e^{-ik_z(z-z')}\mathbf{E}(\mathbf{k}_s; z\backslash z')dz \\ &= \frac{1}{2\pi i}\sum_{\alpha=o,e}\left[\frac{A_{\alpha u}}{k_z - k_{z\alpha}}\mathbf{e}_{\alpha u} - \frac{A_{\alpha d}}{k_z + k_{z\alpha}}\mathbf{e}_{\alpha d}\right]. \qquad (22)\end{aligned}$$

Substituting (21) and (22) into (18), we can obtain

$$\begin{aligned}&\frac{1}{2\pi i}\sum_{\alpha=o,e}\{A_{\alpha u}[(k_z+k_{z\alpha})(\hat{h}\hat{h}+\hat{k}_s\hat{k}_s)-k_s(\hat{z}\hat{k}_s+\hat{k}_s\hat{z})]\cdot\mathbf{e}_{\alpha u} \\ &\qquad - A_{\alpha d}[(k_z-k_{z\alpha})(\hat{h}\hat{h}+\hat{k}_s\hat{k}_s)-k_s(\hat{z}\hat{k}_s+\hat{k}_s\hat{z})]\cdot\mathbf{e}_{\alpha d}\} \\ &= i\omega\mu\mathbf{J}(\mathbf{k}_s, k_z). \qquad (23)\end{aligned}$$

The solutions to the four unknowns $A_{\alpha\beta}$ $(\alpha = o, e; \beta = u, d)$ need four independent equations. Subsequently, we substitute $k_z = \pm k_{z\alpha}$ and premultiply (23) by the characteristic field vectors $\mathbf{e}_{\alpha'\beta'}$. Finally, we get four independent equations for the solutions of $A_{\alpha\beta}$. Considering the uncoupled relationship between the ordinary wave and extraordinary wave, we write the four equations as

$$\mathbf{Q}_{uu}\cdot\mathbf{A}_u = -2\pi\omega\mu\,\Omega_u\cdot\mathbf{S}_u \qquad (24)$$

$$-\mathbf{Q}_{dd}\cdot\mathbf{A}_d = -2\pi\omega\mu\Omega_d\cdot\mathbf{S}_d \qquad (25)$$

where

$$\mathbf{Q}_{\beta\beta} = \begin{bmatrix} Q_{o\beta,o\beta} & 0 \\ 0 & Q_{e\beta,e\beta}\end{bmatrix} \qquad (26)$$

$$\mathbf{A}_\beta = \begin{bmatrix} A_{o\beta} \\ A_{e\beta}\end{bmatrix} \qquad (27)$$

$$\Omega_\beta = \begin{bmatrix} \mathbf{e}_{o\beta} & 0 \\ 0 & \mathbf{e}_{e\beta}\end{bmatrix} \qquad (28)$$

$$\mathbf{S}_\beta = \begin{bmatrix} \mathbf{J}(\mathbf{k}_s, \pm k_{zo}) \\ \mathbf{J}(\mathbf{k}_s, \pm k_{ze})\end{bmatrix} \qquad (29)$$

$$\begin{aligned}Q_{\alpha u,\alpha u} &= -Q_{\alpha d,\alpha d} \\ &= 2k_{z\alpha}\mathbf{e}_{\alpha u}\cdot\mathbf{e}_{\alpha u} - \mathbf{e}_{\alpha u}\cdot(\hat{z}\mathbf{k}_{\alpha u}+\mathbf{k}_{\alpha u}\hat{z})\cdot\mathbf{e}_{\alpha u}. \qquad (30)\end{aligned}$$

Solving (24) and (25) yields

$$\mathbf{A}_\beta = -\pi\omega\mu\,\mathbf{M}_\beta\cdot\Omega_\beta\cdot\mathbf{S}_\beta \qquad (31)$$

with

$$\mathbf{M}_\beta = 2\mathbf{Q}_{\beta\beta}^{-1} = \begin{bmatrix} M_{o\beta,o\beta} & 0 \\ 0 & M_{e\beta,e\beta}\end{bmatrix}. \qquad (32)$$

Substituting (31) into (16) and casting it in a matrix form, we obtain

$$\mathbf{E}(\mathbf{k}_s; z\backslash z') = -\pi\omega\mu\mathbf{P}_\beta^t(z\backslash z')\cdot\mathbf{\Omega}_\beta\cdot\mathbf{M}_\beta\cdot\mathbf{\Omega}_\beta\cdot\mathbf{S}_\beta, \qquad z \neq z' \qquad (33)$$

where

$$\mathbf{P}_\beta(z\backslash z') = \begin{bmatrix} e^{\pm ik_{zo}(z-z')} \\ e^{\pm ik_{ze}(z-z')}\end{bmatrix}. \qquad (34)$$

The electric field in the spatial domain is then expressed by applying the inverse Fourier transform to $\mathbf{E}(\mathbf{k}_s; z\backslash z')$

$$\begin{aligned}\mathbf{E}(\mathbf{r},\mathbf{r}') &= -\pi\omega\mu\int_{-\infty}^{\infty} e^{i\mathbf{k}_s\cdot(\mathbf{r}_s-\mathbf{r}_s')}\mathbf{P}_\beta^t(z\backslash z') \\ &\qquad \cdot\mathbf{\Omega}_\beta\cdot\mathbf{M}_\beta\cdot\mathbf{\Omega}_\beta\cdot\mathbf{S}_\beta\, d\mathbf{k}_s, \qquad \mathbf{r}\neq\mathbf{r}'. \qquad (35)\end{aligned}$$

When $\mathbf{r} = \mathbf{r}'$, the above formulation for the electric field does not exhibit the proper singular behavior. This singular behavior can be captured from the asymptotic behavior of $\mathbf{E}(\mathbf{k})$ when $|k_z| \to \infty$, which is given by

$$\mathbf{E}(\mathbf{k}) \sim \frac{1}{(2\pi)^3}\frac{1}{i\omega\hat{z}\cdot\bar{\bar{\varepsilon}}\cdot\hat{z}}\hat{z}\hat{z}\cdot\hat{a}\delta(z-z'), \qquad |k_z|\to\infty. \qquad (36)$$

Thus, the complete expression for the electric field in the unbounded uniaxial anisotropic medium is represented by

$$\begin{aligned}\mathbf{E}(\mathbf{r},\mathbf{r}') &= \frac{1}{i\omega\hat{z}\cdot\bar{\bar{\varepsilon}}\cdot\hat{z}}\hat{z}\hat{z}\cdot\hat{a}\delta(\mathbf{r}-\mathbf{r}') \\ &\quad - \pi\omega\mu\int_{-\infty}^{\infty} e^{i\mathbf{k}_s\cdot(\mathbf{r}_s-\mathbf{r}_s')}\mathbf{P}_\beta^t(z\backslash z') \\ &\quad \cdot\Omega_\beta\cdot\mathbf{M}_\beta\cdot\mathbf{\Omega}_\beta\cdot\mathbf{S}_\beta\, d\mathbf{k}_s. \qquad (37)\end{aligned}$$

Since the electric field in an unbounded medium relates the dyadic Green's function to the current via

$$\mathbf{E}_n(\mathbf{r}) = \int_{V'} d\mathbf{r}' \mathbf{G}_{nn}(\mathbf{r}, \mathbf{r}') \cdot \mathbf{J}(\mathbf{r}') \tag{38}$$

the formulations of the dyadic Green's function in the unbounded uniaxial anisotropic medium can be derived from (37) in the following explicit form.

For $z > z'$,

$$\mathbf{G}(\mathbf{r}, \mathbf{r}') = \frac{1}{i\omega \hat{z} \cdot \overline{\overline{\varepsilon}} \cdot \hat{z}} \hat{z}\hat{z}\, \delta(\mathbf{r} - \mathbf{r}') - \frac{\omega\mu}{8\pi^2} \int_{-\infty}^{\infty} d\mathbf{k}_s e^{i\mathbf{k}_s \cdot (\mathbf{r}_s - \mathbf{r}_s')} \cdot \left[e^{ik_{zo}(z-z')} \mathbf{e}_{ou} \mathbf{u}_{ou} + e^{ik_{ze}(z-z')} \mathbf{e}_{eu} \mathbf{u}_{eu} \right]. \tag{39}$$

For $z < z'$,

$$\mathbf{G}(\mathbf{r}, \mathbf{r}') = \frac{1}{i\omega \hat{z} \cdot \overline{\overline{\varepsilon}} \cdot \hat{z}} \hat{z}\hat{z}\, \delta(\mathbf{r} - \mathbf{r}') - \frac{\omega\mu}{8\pi^2} \int_{-\infty}^{\infty} d\mathbf{k}_s e^{i\mathbf{k}_s \cdot (\mathbf{r}_s - \mathbf{r}_s')} \cdot \left[e^{-ik_{zo}(z-z')} \mathbf{e}_{od} \mathbf{u}_{od} + e^{-ik_{ze}(z-z')} \mathbf{e}_{ed} \mathbf{u}_{ed} \right] \tag{40}$$

where

$$\mathbf{u}_{o\beta} = M_{o\beta, o\beta} \mathbf{e}_{o\beta} \tag{41}$$

$$\mathbf{u}_{e\beta} = M_{e\beta, e\beta} \mathbf{e}_{e\beta}. \tag{42}$$

III. Dyadic Green's Function for the Planar Multilayered Uniaxial Anisotropic Medium

In this section, based on the boundary condition and the wave iterative technique, the complete and generalized formulations of the spectral-domain Green's function in the planar multilayered uniaxial anisotropic media are explicitly expressed for three cases: viz. $m = n$, $m > n$, and $m < n$, where m and n denote the layers that the source point and observation point are located inside, respectively. The geometry of the general planar multilayered uniaxial anisotropic medium is depicted in Fig. 1.

A. Local Reflection and Transmission Matrices

To satisfy the boundary conditions of the continuity of the tangential electric and magnetic fields, the tangential components of $\mathbf{E}$ and $\mathbf{H}$ along the $\hat{h}$ and $\hat{k}_s$ directions are matched at the interface of two layers

$$\mathbf{X}_\beta^{(m)} + \mathbf{X}_{\overline{\beta}}^{(m)} \cdot \mathbf{R}_{m,n}^{(\beta)} = \mathbf{X}_\beta^{(n)} \cdot \mathbf{T}_{m,n}^{(\beta)} \tag{43}$$

$$\mathbf{Y}_\beta^{(m)} + \mathbf{Y}_{\overline{\beta}}^{(m)} \cdot \mathbf{R}_{m,n}^{(\beta)} = \mathbf{Y}_\beta^{(n)} \cdot \mathbf{T}_{m,n}^{(\beta)} \tag{44}$$

where $\mathbf{R}_{m,n}^{\beta}$ is the local reflection matrix and $\mathbf{T}_{m,n}^{\beta}$ is the local transmission matrix. The character $\beta = u$ ($\overline{\beta} = d$) for $m > n$ and $\beta = d$ ($\overline{\beta} = u$) for $m < n$

$$\mathbf{R}_{m,n}^{\beta} = \begin{bmatrix} R_{mn}^o & 0 \\ 0 & R_{mn}^e \end{bmatrix} \tag{45}$$

$$\mathbf{T}_{m,n}^{\beta} = \begin{bmatrix} T_{mn}^o & 0 \\ 0 & T_{mn}^e \end{bmatrix} \tag{46}$$

$$\mathbf{X}_\beta^{(m)} = \begin{bmatrix} \hat{h} \cdot \mathbf{e}_{o\beta}^{(m)} & \hat{h} \cdot \mathbf{e}_{e\beta}^{(m)} \\ \hat{k}_s \cdot \mathbf{e}_{o\beta}^{(m)} & \hat{k}_s \cdot \mathbf{e}_{e\beta}^{(m)} \end{bmatrix} \tag{47}$$

$$\mathbf{Y}_\beta^{(m)} = \begin{bmatrix} \hat{h} \cdot \mathbf{h}_{o\beta}^{(m)} & \hat{h} \cdot \mathbf{h}_{e\beta}^{(m)} \\ \hat{k}_s \cdot \mathbf{h}_{o\beta}^{(m)} & \hat{k}_s \cdot \mathbf{h}_{e\beta}^{(m)} \end{bmatrix}. \tag{48}$$

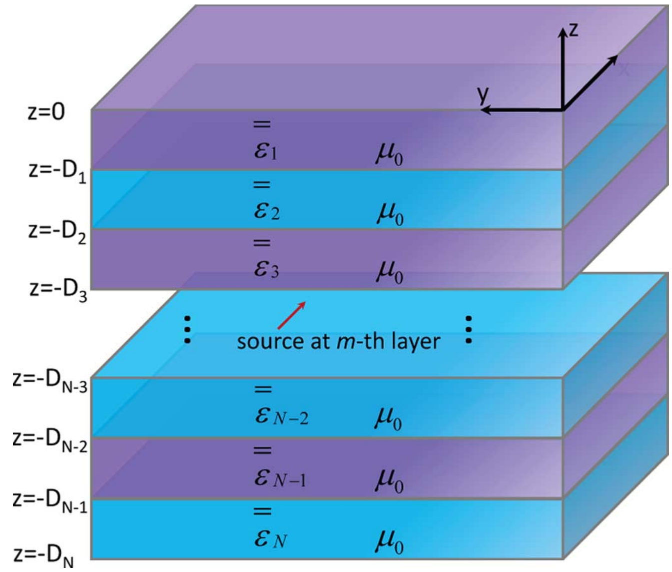

Fig. 1. Geometry of the general planar multilayered uniaxial anisotropic medium.

R_{mn}^{α} is the local reflection coefficient when the incident plane wave is in region m; T_{mn}^{α} is the local transmission coefficient from region m to region n.

Derived from the (43) and (44), the reflection and transmission matrices can be expressed as

$$\mathbf{R}_{m,n}^{(\beta)} = \left[\mathbf{X}_{\overline{\beta}}^{(m)} - \mathbf{X}_\beta^{(n)} \cdot \{\mathbf{Y}_\beta^{(n)}\}^{-1} \cdot \mathbf{Y}_{\overline{\beta}}^{(m)} \right]^{-1} \cdot \left[-\mathbf{X}_\beta^{(m)} + \mathbf{X}_\beta^{(n)} \cdot \{\mathbf{Y}_\beta^{(n)}\}^{-1} \cdot \mathbf{Y}_\beta^{(m)} \right] \tag{49}$$

$$\mathbf{T}_{m,n}^{(\beta)} = \left[\mathbf{Y}_\beta^{(n)} - \mathbf{Y}_{\overline{\beta}}^{(m)} \cdot \{\mathbf{X}_{\overline{\beta}}^{(m)}\}^{-1} \cdot \mathbf{X}_\beta^{(n)} \right]^{-1} \cdot \left[\mathbf{Y}_\beta^{(m)} - \mathbf{Y}_{\overline{\beta}}^{(m)} \cdot \{\mathbf{X}_{\overline{\beta}}^{(m)}\}^{-1} \cdot \mathbf{X}_\beta^{(m)} \right]. \tag{50}$$

B. Global Reflection and Transmission Matrices

Due to multiple reflections and cross-polarization effects, the electric field in an arbitrary layer n is represented in terms of upward propagating and downward propagating waves as follows:

$$\mathbf{E}_n(z_n) \equiv \mathbf{E}(\mathbf{k}_s; z_n) = f_n^o \mathbf{e}_{ou}^{(n)} e^{ik_{zo}^{(n)} z_n} + f_n^e \mathbf{e}_{eu}^{(n)} e^{ik_{ze}^{(n)} z_n} + g_n^o \mathbf{e}_{od}^{(n)} e^{-ik_{zo}^{(n)} z_n} + g_n^e \mathbf{e}_{ed}^{(n)} e^{-ik_{ze}^{(n)} z_n} \tag{51}$$

which can be cast in the following matrix form:

$$\mathbf{E}_n(z_n) = \mathbf{G}_u^{(n)}(z_n) \cdot \mathbf{f}_n + \mathbf{G}_d^{(n)}(z_n) \cdot \mathbf{g}_n \tag{52}$$

where

$$\mathbf{G}_u^{(n)}(z_n) = \begin{bmatrix} e^{ik_{zo}^{(n)} z_n} & 0 \\ 0 & e^{ik_{ze}^{(n)} z_n} \end{bmatrix} \tag{53}$$

$$\mathbf{G}_d^{(n)}(z_n) = \begin{bmatrix} e^{-ik_{zo}^{(n)} z_n} & 0 \\ 0 & e^{-ik_{ze}^{(n)} z_n} \end{bmatrix} \tag{54}$$

$$\mathbf{f}_n = \begin{bmatrix} f_n^o \\ f_n^e \end{bmatrix} \tag{55}$$

$$\mathbf{g}_n = \begin{bmatrix} g_n^o \\ g_n^e \end{bmatrix}. \tag{56}$$

$\mathbf{G}_u^{(n)}(z_n)$ represents the upward propagating wave expressed in the $[\mathbf{e}_{ou}^{(n)}, \mathbf{e}_{eu}^{(n)}]$ coordinate system. The first component on the diagonal of $\mathbf{G}_u^{(n)}(z_n)$ is along $\mathbf{e}_{ou}^{(n)}$ and the second component on the diagonal is along $\mathbf{e}_{eu}^{(n)}$. Similarly, $\mathbf{G}_d^{(n)}(z_n)$ represents the downward propagating wave expressed in the $[\mathbf{e}_{od}^{(n)}, \mathbf{e}_{ed}^{(n)}]$ coordinate system. In the layer $n-1$, the electric field vector is expressed by

$$\mathbf{E}_{n-1}(z_{n-1}) = \mathbf{G}_u^{(n-1)}(z_{n-1}) \cdot \mathbf{f}_{n-1} + \mathbf{G}_d^{(n-1)}(z_{n-1}) \cdot \mathbf{g}_{n-1}. \tag{57}$$

At the interface of layer $n-1$ and layer n, the upward global reflection and transmission matrices are related with the fields by the following relationships:

$$\begin{aligned}\mathbf{G}_d^{(n)}&(z_n = -D_{n-1}) \cdot \mathbf{g}_n \\ &= \mathbf{R}_{Un} \cdot \mathbf{G}_u^{(n)}(z_n = -D_{n-1}) \cdot \mathbf{f}_n \end{aligned}\tag{58}$$

$$\begin{aligned}\mathbf{T}_{Un} &\cdot \mathbf{G}_u^{(n)}(z_n = -D_{n-1}) \cdot \mathbf{f}_n \\ &= \mathbf{G}_u^{(n-1)}(z_{n-1} = -D_{n-1}) \cdot \mathbf{f}_{n-1}\end{aligned}\tag{59}$$

where $\mathbf{R}_{Un}$ and $\mathbf{T}_{Un}$ are the global reflection matrix and global transmission matrix from layer n to layer $n-1$, respectively. It is noted that the downward propagating wave in the layer n is a consequence of the transmission of the downward propagating wave in the layer $n-1$ in combination with the reflection of the upward propagating wave in the layer n. Thus, at the interface $z = -D_{n-1}$, the constraint condition is

$$\begin{aligned}\mathbf{R}_{Un} &\cdot \mathbf{G}_u^{(n)}(z_n = -D_{n-1}) \cdot \mathbf{f}_n \\ &= \mathbf{R}_{n,n-1}^{(u)} \cdot \mathbf{G}_u^{(n)}(z_n = -D_{n-1}) \cdot \mathbf{f}_n \\ &\quad + \mathbf{T}_{n-1,n}^{d} \cdot \mathbf{G}_d^{(n-1)}(z_n = -D_{n-1}) \cdot \mathbf{g}_{n-1}.\end{aligned}\tag{60}$$

By using the expression of $\mathbf{g}_n$ from (58), we can write (60) as

$$\begin{aligned}\mathbf{R}_{Un} &\cdot \mathbf{G}_u^{(n)}(z_n = -D_{n-1}) \cdot \mathbf{f}_n \\ &= \mathbf{R}_{n,n-1}^{(u)} \cdot \mathbf{G}_u^{(n)}(z_n = -D_{n-1}) \cdot \mathbf{f}_n + \mathbf{T}_{n-1,n}^{d} \\ &\quad \cdot \mathbf{G}_d^{(n-1)}(z_n = -D_{n-1}) \\ &\quad \cdot \mathbf{G}_d^{(n-1)}(z_{n-1} = -D_{n-2})^{-1} \\ &\quad \cdot \mathbf{R}_{Un-1} \cdot \mathbf{G}_u^{(n-1)}(z_{n-1} = -D_{n-2}) \cdot \mathbf{f}_{n-1}.\end{aligned}\tag{61}$$

Next, we notice that the upward propagating wave in the layer $n-1$ is a superposition of the reflection of the downward propagating wave in the layer $n-1$ and the transmission of the upward propagating wave in the layer n. At the interface $z = -D_{n-1}$, we have the constraint condition

$$\begin{aligned}\mathbf{G}_u^{(n-1)}&(z_{n-1} = -D_{n-1}) \cdot \mathbf{f}_{n-1} \\ &= \mathbf{T}_{n,n-1}^{(n)} \cdot \mathbf{G}_u^{(n)}(z_n = -D_{n-1}) \cdot \mathbf{f}_n \\ &\quad + \mathbf{R}_{n-1,n}^{(d)} \cdot \mathbf{G}_d^{(n-1)}(z_{n-1} = -D_{n-1}) \cdot \mathbf{g}_{n-1}.\end{aligned}\tag{62}$$

Substituting the expression of g_{n-1} from (58), we can write (62) as

$$\begin{aligned}\mathbf{G}_u^{(n-1)}&(z_{n-1} = -D_{n-1}) \cdot \mathbf{f}_{n-1} \\ &= \mathbf{T}_{n,n-1}^{(n)} \cdot \mathbf{G}_u^{(n)}(z_n = -D_{n-1}) \cdot \mathbf{f}_n \\ &\quad + \mathbf{R}_{n-1,n}^{(d)} \cdot \mathbf{G}_d^{(n-1)}(z_{n-1} = -D_{n-1}) \\ &\quad \cdot \mathbf{G}_d^{(n-1)}(z_{n-1} = -D_{n-2})^{-1} \\ &\quad \cdot \mathbf{R}_{Un-1} \cdot \mathbf{G}_u^{(n-1)}(z_{n-1} = -D_{n-2}) \cdot \mathbf{f}_{n-1}.\end{aligned}\tag{63}$$

From (61) and (63), we finally get the following recursive expression for the upward global reflection matrix:

$$\begin{aligned}\mathbf{R}_{Un} = &\mathbf{R}_{n,n-1}^{(u)} + \mathbf{T}_{n-1,n}^{(d)} \cdot \mathbf{G}_d^{(n-1)}(z_{n-1} = -D_{n-1} + D_{n-2}) \\ &\cdot \mathbf{R}_{Un-1} \cdot \mathbf{G}_u^{(n-1)}(z_{n-1} = -D_{n-2} + D_{n-1}) \\ &\cdot \Big[\mathbf{I} - \mathbf{R}_{n-1,n}^{(d)} \cdot \mathbf{G}_d^{(n-1)}(z_{n-1} = -D_{n-1} + D_{n-2}) \\ &\quad \cdot \mathbf{R}_{Un-1} \cdot \mathbf{G}_u^{(n-1)}(z_{n-1} = -D_{n-2} + D_{n-1})\Big]^{-1} \\ &\cdot \mathbf{T}_{n,n-1}^{(u)}.\end{aligned}\tag{64}$$

Similarly, the recursive formulation of the downward global reflection matrix is derived as follows:

$$\begin{aligned}\mathbf{R}_{Dn} = &\mathbf{R}_{n,n+1}^{(d)} + \mathbf{T}_{n+1,n}^{(u)} \cdot \mathbf{G}_u^{(n+1)}(z_{n+1} = -D_n + D_{n+1}) \\ &\cdot \mathbf{R}_{Dn+1} \cdot \mathbf{G}_u^{(n+1)}(z_{n+1} = -D_{n+1} + D_n) \\ &\cdot \Big[\mathbf{I} - \mathbf{R}_{n+1,n}^{(u)} \cdot \mathbf{G}_u^{(n+1)}(z_{n+1} = -D_n + D_{n+1}) \\ &\quad \cdot \mathbf{R}_{Dn+1} \cdot \mathbf{G}_d^{(n+1)}(z_{n+1} = -D_{n+1} + D_n)\Big]^{-1} \\ &\cdot \mathbf{T}_{n,n+1}^{(d)}.\end{aligned}\tag{65}$$

From (59) and (63), the recursive expression for the upward global transmission matrix is given by

$$\begin{aligned}\mathbf{T}_{Un} = &\Big[\mathbf{I} - \mathbf{R}_{n-1,n}^{(d)} \cdot \mathbf{G}_d^{(n-1)}(z_{n-1} = -D_{n-1} + D_{n-2}) \\ &\quad \cdot \mathbf{R}_{Un-1} \cdot \mathbf{G}_u^{(n-1)}(z_{n-1} = -D_{n-2} + D_{n-1})\Big]^{-1} \\ &\cdot \mathbf{T}_{n,n-1}^{(u)}.\end{aligned}\tag{66}$$

Similarly, the downward global transmission matrix can be expressed as

$$\begin{aligned}\mathbf{T}_{Dn} = &\Big[\mathbf{I} - \mathbf{R}_{n+1,n}^{(u)} \cdot \mathbf{G}_u^{(n+1)}(z_{n+1} = -D_n + D_{n+1}) \\ &\quad \cdot \mathbf{R}_{Dn+1} \cdot \mathbf{G}_d^{(n+1)}(z_{n+1} = -D_{n+1} + D_n)\Big]^{-1} \\ &\cdot \mathbf{T}_{n,n+1}^{(d)}.\end{aligned}\tag{67}$$

C. Dyadic Green's Function for the Case $m = n$

For the case where the source and observation points are in the same layer n, based on the Fourier transform, the electric field can be expressed as

$$\mathbf{E}_n(\mathbf{r}) = \int_{-\infty}^{\infty} d\mathbf{k}_s e^{i\mathbf{k}_s \cdot (\mathbf{r}_s - \mathbf{r}_s')} \mathbf{E}_n(\mathbf{k}_s; z) \tag{68}$$

where

$$\mathbf{E}_n(\mathbf{k}_s; z) = e^{ik_{zo}^{(n)}|z-z'|} \mathbf{e}_{o\beta}^{(n)} S_{o\beta}^{(n)} + e^{ik_{ze}^{(n)}|z-z'|} \mathbf{e}_{e\beta}^{(n)} S_{e\beta}^{(n)} \tag{69}$$

$$S_{\alpha\beta}^{(n)} = -\frac{\omega\mu_n}{8\pi^2} \mathbf{u}_{\alpha\beta}^{(n)} \cdot \hat{a}. \tag{70}$$

Based on (37), $\mathbf{E}_n(\mathbf{k}_s;z)$ can be cast as follows:

$$\mathbf{E}_n(\mathbf{k}_s;z) = \mathbf{G}_\beta^{(n)}(z)\cdot\mathbf{G}_\beta^{(n)}(-z')\cdot\mathbf{S}_\beta^{(n)} \tag{71}$$

where

$$\mathbf{S}_\beta^{(n)} = \begin{bmatrix} S_o^{(n)} \\ S_e^{(n)} \end{bmatrix} = -\frac{\omega\mu_n}{8\pi^2}\begin{bmatrix} \mathbf{u}_{o\beta}^{(n)} \\ \mathbf{u}_{e\beta}^{(n)} \end{bmatrix}\cdot\hat{a}. \tag{72}$$

In an arbitrary layer n, the electric field is written as

$$\mathbf{E}_n(\mathbf{k}_s;z_n) = \mathbf{G}_\beta^{(n)}(z_n)\cdot\mathbf{G}_\beta^{(n)}(-z'_n)\cdot\mathbf{S}_\beta^{(n)} + \mathbf{G}_u^{(n)}(z_n)\cdot\mathbf{f}_n + \mathbf{G}_d^{(n)}(z_n)\cdot\mathbf{g}_n \tag{73}$$

where two unknown vectors, $\mathbf{f}_n$ and $\mathbf{g}_n$, need to be determined. For $z_n > z'_n$,

$$\mathbf{E}_n(\mathbf{k}_s;z_n) = \mathbf{G}_u^{(n)}(z_n)\cdot\left[\mathbf{G}_u^{(n)}(-z'_n)\cdot\mathbf{S}_u^{(n)} + \mathbf{f}_n\right] + \mathbf{G}_d^{(n)}(z_n)\cdot\mathbf{g}_n \tag{74}$$

where the first term represents waves propagating upward and the second term represents waves propagating downward. At the interface $z = -D_{n-1}$, the downward propagating waves are related to the upward propagating waves by the upward global reflection matrix

$$\mathbf{g}_n = \mathbf{G}_d^{(n)^{-1}}(z_n = -D_{n-1})\cdot\mathbf{R}_{Un}\cdot\mathbf{G}_u^{(n)}(z_n=-D_{n-1})\cdot\left[\mathbf{G}_u^{(n)}(-z')\cdot\mathbf{S}_u^{(n)} + \mathbf{f}_n\right]. \tag{75}$$

Similarly, for $z_n < z'_n$,

$$\mathbf{E}_n(\mathbf{k}_s;z_n) = \mathbf{G}_d^{(n)}(z_n)\cdot\left[\mathbf{G}_d^{(n)}(-z'_n)\cdot\mathbf{S}_d^{(n)} + \mathbf{g}_n\right] + \mathbf{G}_u^{(n)}(z_n)\cdot\mathbf{f}_n \tag{76}$$

$$\mathbf{f}_n = \mathbf{G}_u^{(n)^{-1}}(z_n=-D_n)\cdot\mathbf{R}_{Dn}\mathbf{G}_d^{(n)}(z_n=-D_n)\cdot\left[\mathbf{G}_d^{(n)}(-z')\cdot\mathbf{S}_d^{(n)} + \mathbf{g}_n\right]. \tag{77}$$

Solving for $\mathbf{f}_n$ and $\mathbf{g}_n$ from (75) and (77), we obtain

$$\begin{aligned}\mathbf{g}_n = {} & \mathbf{G}_d^{(n)^{-1}}(z_n=-D_{n-1})\cdot\mathbf{R}_{Un}\cdot\mathbf{M}_n \\ & \cdot\mathbf{G}_u^{(n)}(z_n=-D_{n-1}) \\ & \cdot\left[\mathbf{G}_u^{(n)}(-z')\cdot\mathbf{S}_u^{(n)} + \mathbf{G}_u^{(n)}(z_n=D_n)\cdot\mathbf{R}_{Dn}\right. \\ & \left.\cdot\mathbf{G}_d^{(n)}(z_n=-D_n)\cdot\mathbf{G}_d^{(n)}(-z')\cdot\mathbf{S}_d^{(n)}\right]\end{aligned} \tag{78}$$

$$\begin{aligned}\mathbf{f}_n = {} & \mathbf{G}_u^{(n)^{-1}}(z_n=-D_n)\cdot\mathbf{R}_{Dn}\cdot\mathbf{N}_n \\ & \cdot\mathbf{G}_d^{(n)}(z_n=-D_n) \\ & \cdot\left[\mathbf{G}_d^{(n)}(-z')\cdot\mathbf{S}_d^{(n)} + \mathbf{G}_d^{(n)}(z_n=D_{n-1})\cdot\mathbf{R}_{Un}\right. \\ & \left.\cdot\mathbf{G}_u^{(n)}(z_n=-D_{n-1})\cdot\mathbf{G}_u^{(n)}(-z')\cdot\mathbf{S}_u^{(n)}\right]\end{aligned} \tag{79}$$

where

$$\mathbf{M}_n = \left[\mathbf{I} - \mathbf{G}_u^{(n)}(z_n=-D_{n-1}+D_n)\cdot\mathbf{R}_{Dn}\cdot\mathbf{G}_d^{(n)}(z_n=-D_n+D_{n-1})\cdot\mathbf{R}_{Un}\right]^{-1} \tag{80}$$

$$\mathbf{N}_n = \left[\mathbf{I} - \mathbf{G}_d^{(n)}(z_n=-D_n+D_{n-1})\cdot\mathbf{R}_{Un}\cdot\mathbf{G}_u^{(n)}(z_n=-D_{n-1}+D_n)\cdot\mathbf{R}_{Dn}\right]^{-1}. \tag{81}$$

Substituting (78) and (79) into (73), we get the following expression for the electric field:

$$\begin{aligned}\mathbf{E}_n(\mathbf{k}_s;z_n) = {} & \mathbf{G}_\beta^{(n)}(z_n)\cdot\mathbf{G}_\beta^{(n)}(-z'_n)\cdot\mathbf{S}_\beta^{(n)} \\ & + \mathbf{G}_u^{(n)}(z_n)\cdot\mathbf{G}_u^{(n)^{-1}}(z_n=-D_n) \\ & \cdot\mathbf{R}_{Dn}\cdot\mathbf{N}_n\cdot\mathbf{G}_d^{(n)}(z_n=-D_n) \\ & \cdot\left[\mathbf{G}_d^{(n)}(-z')\cdot\mathbf{S}_d^{(n)} + \mathbf{G}_d^{(n)}(z_n=D_{n-1})\cdot\mathbf{R}_{Un}\right. \\ & \left.\cdot\mathbf{G}_u^{(n)}(z_n=-D_{n-1})\cdot\mathbf{G}_u^{(n)}(-z')\cdot\mathbf{S}_u^{(n)}\right] \\ & + \mathbf{G}_d^{(n)}(z_n)\cdot\mathbf{G}_d^{(n)^{-1}}(z_n=-D_{n-1}) \\ & \cdot\mathbf{R}_{Un}\cdot\mathbf{M}_n\cdot\mathbf{G}_u^{(n)}(z_n=-D_{n-1}) \\ & \cdot\left[\mathbf{G}_u^{(n)}(-z')\cdot\mathbf{S}_u^{(n)} + \mathbf{G}_u^{(n)}(z_n=D_n)\cdot\mathbf{R}_{Dn}\right. \\ & \left.\cdot\mathbf{G}_d^{(n)}(z_n=-D_n)\cdot\mathbf{G}_d^{(n)}(-z')\cdot\mathbf{S}_d^{(n)}\right].\end{aligned} \tag{82}$$

Here, $\beta = u$ for $z_n > z'_n$ and $\beta = d$ for $z_n < z'_n$. Based on (38) and (82), the dyadic Green's function in the planar multilayered uniaxial anisotropic medium is given in the Appendix for the case of $m = n$.

D. Dyadic Green's Function for the Case $m \neq n$

First, the case $m > n$ is considered. The source point is located inside the layer m and the observation point is located inside the layer n. The electric field in the layer m is expressed as

$$\mathbf{E}_m(\mathbf{k}_s;z_m) = \left[\mathbf{G}_u^m(z_m+D_{m-1}) + \mathbf{G}_d^{(m)}(z_m)\cdot\mathbf{G}_d^{(m)^{-1}}(z_m=-D_{m-1})\cdot\mathbf{R}_{Um}\right]\cdot\mathbf{e}^m(z'_m) \tag{83}$$

where

$$\begin{aligned}\mathbf{e}^m(z'_m) = {} & \mathbf{M}_m\cdot\mathbf{G}_u^{(m)}(z_m=-D_{m-1}) \\ & \cdot\left[\mathbf{G}_u^{(m)}(-z'_m)\cdot\mathbf{S}_u^{(m)} + \mathbf{G}_u^{(m)}(z_m=D_m)\right. \\ & \left.\cdot\mathbf{R}_{Dm}\cdot\mathbf{G}_d^{(m)}(z_m=-D_m-z'_m)\cdot\mathbf{S}_d^{(m)}\right].\end{aligned} \tag{84}$$

In the layer $m-1$, the electric field can be represented as follows:

$$\mathbf{E}_{m-1}(\mathbf{k}_s;z_{m-1}) = \mathbf{G}_u^{m-1}(z_{m-1})\cdot\mathbf{f}_{m-1} + \mathbf{G}_d^{(m-1)}(z_{m-1})\cdot\mathbf{g}_{m-1}. \tag{85}$$

At the interface $z = -D_{m-2}$, the downward propagating wave is related to the upward propagating wave by the upward global reflection matrix $\mathbf{R}_{Um-1}$. This yields

$$\mathbf{g}_{m-1} = \mathbf{G}_d^{(m-1)^{-1}}(z_{m-1}=-D_{m-2})\cdot\mathbf{R}_{Um-1}\cdot\mathbf{G}_u^{(m-1)}(z_{m-1}=-D_{m-2})\cdot\mathbf{f}_{m-1}. \tag{86}$$

At the interface $z = -D_{m-1}$, the upward propagating wave in the layer $m-1$ is related to the upward propagating wave in the layer m by the upward global transmission matrix $\mathbf{T}_{Um}$, i.e.,

$$\mathbf{T}_{Um} \cdot \mathbf{G}_u^{(m)}(z_m = -D_{m-1}) \cdot \mathbf{e}^{(m)}(z'_m) = \mathbf{G}_u^{(m-1)}(z_{m-1} = -D_{m-1}) \cdot \mathbf{f}_{m-1} \quad (87)$$

which yields

$$\mathbf{f}_{m-1} = \mathbf{G}_u^{(m-1)^{-1}}(z_{m-1} = -D_{m-1}) \cdot \mathbf{T}_{Um} \cdot \mathbf{G}_u^{(m)}(z_m = -D_{m-1}) \cdot \mathbf{e}^{(m)}(z'_m). \quad (88)$$

Thus, the electric field in the layer $m-1$ is represented as

$$\begin{aligned}\mathbf{E}_{m-1}(\mathbf{k}_s; z_{m-1}) &= \Big[\mathbf{G}_u^{(m-1)}(z_{m-1}) + \mathbf{G}_d^{(m-1)}(z_{m-1}) \\ &\quad \cdot \mathbf{G}_d^{(m-1)^{-1}}(z_{m-1} = -D_{m-2}) \cdot \mathbf{R}_{Um-1} \\ &\quad \cdot \mathbf{G}_u^{(m-1)}(z_{m-1} = -D_{m-2})\Big] \\ &\quad \cdot \mathbf{G}_u^{(m-1)^{-1}}(z_{m-1} = -D_{m-1}) \cdot \mathbf{T}_{Um} \\ &\quad \cdot \mathbf{G}_u^{(m)}(z_m = -D_{m-1}) \cdot \mathbf{e}^{m}(z'_m). \end{aligned} \quad (89)$$

Finally, the electric field in an arbitrary layer n above the source layer m is given by

$$\begin{aligned}\mathbf{E}_n(\mathbf{k}_s; z_n) = \Big[&\mathbf{G}_u^{(n)}(z_n) + \mathbf{G}_d^{(n)}(z_n) \cdot \mathbf{G}_d^{(n)^{-1}}(z_n = -D_{n-1}) \\ &\cdot \mathbf{R}_{Un} \cdot \mathbf{G}_u^{(n)}(z_n = -D_{n-1})\Big] \\ &\cdot \mathbf{G}_u^{(n)^{-1}}(z_n = -D_n) \cdot \mathbf{Y}_{m,n}^{(u)} \\ &\cdot \mathbf{G}_u^{(m)}(z_m = -D_{m-1}) \cdot \mathbf{e}^{m}(z'_m) \end{aligned} \quad (90)$$

where $\mathbf{Y}_{m,n}^{(u)}$ is the global transmission matrix from the layer m to the layer n and its expression is given by

$$\begin{aligned}\mathbf{Y}_{m,n}^{(u)} = \mathbf{T}_{Un+1} &\cdot \mathbf{G}_u^{(n+1)}(z_{n+1} = -D_n + D_{n+1}) \\ &\cdot \mathbf{T}_{Un+2} \cdot \cdots \cdot \mathbf{G}_u^{(m-1)}(z_{m-1} = -D_{m-2} + D_{m-1}) \\ &\cdot \mathbf{T}_{Um}. \end{aligned} \quad (91)$$

Hence, substituting the formulation of $\mathbf{e}^m(z'_m)$, we get the explicit expression of $\mathbf{E}_n(\mathbf{k}_s; z_n)$ for the case of $m > n$,

$$\begin{aligned}\mathbf{E}_n(\mathbf{k}_s; z_n) = \Big[&\mathbf{G}_u^{(n)}(z_n + D_n) + \mathbf{G}_d^{(n)}(z_n + D_{n-1}) \cdot \mathbf{R}_{Un} \\ &\cdot \mathbf{G}_u^{(n)}(z_n = -D_{n-1} + D_n)\Big] \cdot \mathbf{Y}_{m,n}^{(u)} \cdot \mathbf{M}_m \\ &\cdot \Big[\mathbf{G}_u^{(m)}(z_m = -D_{m-1} - z'_m) \cdot \mathbf{S}_u^{(m)} \\ &\quad + \mathbf{G}_u^{(m)}(z_m = -D_{m-1} + D_m) \cdot \mathbf{R}_{Dm} \\ &\quad \cdot \mathbf{G}_d^{(m)}(z_m = -D_m - z'_m) \cdot \mathbf{S}_d^{(m)}\Big]. \end{aligned} \quad (92)$$

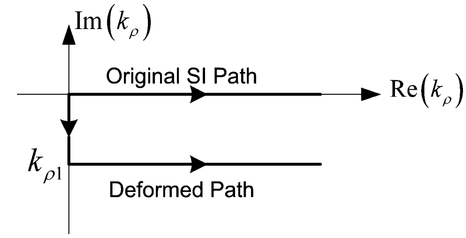

Fig. 2. Deformed SIP.

For the case of $m < n$, following the same derivation process as employed earlier for the case of $m > n$, we get the expression for the electric field in the layer n as follows:

$$\begin{aligned}\mathbf{E}_n(\mathbf{k}_s; z_n) = \Big[&\mathbf{G}_d^{(n)}(z_n + D_{n-1}) + \mathbf{G}_u^{(n)}(z_n + D_n) \cdot \mathbf{R}_{Dn} \\ &\cdot \mathbf{G}_d^{(n)}(z_n = -D_n + D_{n-1})\Big] \cdot \mathbf{Y}_{mn}^{(d)} \cdot \mathbf{N}_m \\ &\cdot \Big[\mathbf{G}_d^{(m)}(z_m = -D_m - z'_m) \cdot \mathbf{S}_d^{(m)} \\ &\quad + \mathbf{G}_d^{(m)}(z_m = -D_m + D_{m-1}) \cdot \mathbf{R}_{Um} \\ &\quad \cdot \mathbf{G}_u^{(m)}(z_m = -D_{m-1} - z'_m) \cdot \mathbf{S}_u^{(m)}\Big]. \end{aligned} \quad (93)$$

A complete and generalized set of the dyadic Green's function in the planar multilayered uniaxial anisotropic media has been derived in the spectral domain. The important point to note is that the formulations of Green's function are independent of the choice of the coordinate system. Hence, they are applicable to general multilayered structures without any accompanying requirement for coordinate change, which is the primary shortcoming in [23]. Similar expressions can be easily obtained for the dyadic Green's function for the magnetic field $\Gamma(\mathbf{r}, \mathbf{r}')$ due to an arbitrary oriented electric current point source and the dyadic Green's functions for the electric field $\mathbf{G}_m(\mathbf{r}, \mathbf{r}')$ and the magnetic field $\Gamma_m(\mathbf{r}, \mathbf{r}')$ due to an arbitrary oriented magnetic current point source. From the three formulations (111), (118), (123), it is clearly shown that the dyadic Green's functions in the spatial domain are expressed in terms of the cumbersome Sommerfeld integrals. To expedite the calculation of the Sommerfeld integrals, the newly developed MFHT method is employed to calculate the dyadic Green's functions.

IV. MFHT Method

In this section, an MFHT filter algorithm is introduced to calculate the dyadic Green's function for general multilayered geometries. In order to move away from the surface wave poles and the branch points to obtain the smooth spectrum of Green's function, the Sommerfeld integration path (SIP) is deformed from the real axis to the fourth quadrant, as shown in Fig. 2. The Sommerfeld integral can then be written as

$$G(r, r') = \frac{1}{2\pi}\int_0^{jk_{\rho 1}} \widetilde{G}(k_\rho; z, z') J_n(k_\rho \rho) k_\rho^{n+1} dk_\rho + \frac{1}{2\pi}\int_{jk_{\rho 1}}^{\infty + jk_{\rho 1}} \widetilde{G}(k_\rho; z, z') J_n(k_\rho \rho) k_\rho^{n+1} dk_\rho \quad (94)$$

where $k_{\rho 1}$ is a real number. The first integral can be efficiently calculated by the adaptive Simpson quadrature method with a computational time quite small compared with the total computational time. The second integral is evaluated by the MFHT method and it can be written as

$$\begin{aligned} G_2(\rho) &= \frac{1}{2\pi}\int_{jk_{\rho 1}}^{\infty+jk_{\rho 1}} \widetilde{G}(k_\rho; z, z') J_n(k_\rho \rho) k_\rho^{n+1} dk_\rho \\ &= \frac{1}{2\pi}\int_0^{\infty} \widetilde{G}'(k'_\rho; z, z') J_n(k'_\rho \rho + jk_{\rho 1}\rho) dk'_\rho \end{aligned} \quad (95)$$

with

$$k'_\rho = k_\rho - jk_{\rho 1} \quad (96)$$

$$\widetilde{G}'(k'_\rho; z, z') = \widetilde{G}(k_\rho; z, z') \cdot k_\rho^{n+1} \quad (97)$$

where $\rho > 0$ and the input function $\widetilde{G}'$ is a complex function of the real argument k'_ρ. Although the input function of this integral becomes a smooth function along the deformed integration path, the argument of the Bessel function becomes complex. Since the FHT filters developed thus far only permit the argument of Bessel function in the Hankel integral to be real, the traditional FHT method is not directly applicable here.

In order to use the FHT method, a Bessel function with a complex argument can be expressed as [29]

$$J_n(u \pm v) = \sum_{k=-\infty}^{\infty} J_{n\mp k}(u) J_k(v). \quad (98)$$

The two arguments, u and v, can be arbitrary values and the Bessel functions with complex arguments in (95) are expanded by the sum

$$J_n(k'_\rho \rho + jk_{\rho 1}\rho) = \sum_{k=-\infty}^{\infty} J_{n-k}(jk_{\rho 1}\rho) J_k(k'_\rho \rho) \quad (99)$$

so that (95) can be written as

$$\begin{aligned} G_2(\rho) &= \frac{1}{2\pi}\int_0^{\infty} \widetilde{G}'(k'_\rho; z, z') J_n(k'_\rho \rho + jk_{\rho 1}\rho) dk'_\rho \\ &= \frac{1}{2\pi}\sum_{k=-\infty}^{\infty} J_{n-k}(jk_{\rho 1}\rho) \int_0^{\infty} \widetilde{G}'(k'_\rho; z, z') J_k(k'_\rho \rho) dk'_\rho \end{aligned} \quad (100)$$

where

$$J_m(jk_{\rho 1}\rho) = e^{jm\pi/2} \cdot I_m(k_{\rho 1}\rho) = j^m \cdot I_m(k_{\rho 1}\rho). \quad (101)$$

The modified Bessel function I_m is a monotonic increasing function. Each expansion term in (100) can be efficiently and accurately evaluated by the traditional FHT method. In this paper, we choose the optimized FHT filter method proposed by [30] to calculate the Hankel integrals since the FHT coefficients for the Hankel transform with an arbitrary order can be easily obtained.

In the optimized FHT filter technique, we introduce two functions, which are related via the functions in (100)

$$h(k'_\rho) = \widetilde{G}'(k'_\rho; z, z') \quad (102)$$

$$H(\rho) = \rho \cdot G_2(\rho) \cdot 2\pi \cdot [J_k(jk_{\rho 1}\rho)]^{-1}. \quad (103)$$

Each expansion term in (100) can then be rewritten as

$$H(\rho) \cdot \rho^{-1} = \int_0^{\infty} h(k'_\rho) \cdot J_{n-k}(k'_\rho \rho) dk'_\rho. \quad (104)$$

Equation (104) is transformed to a linear convolution-type integral by using the substitutions $x = \ln(\rho)$ and $y = \ln(1/k'_\rho)$

$$H(e^x) \cdot e^{-x} = \int_{-\infty}^{\infty} h(e^{-y}) \cdot [e^{-y} \cdot J_{n-k}(e^{x-y})] dy \quad (105)$$

where h is the input function related with the spectral-domain Green's function, H is the output function related with the spatial-domain Green's function, and the product in the bracket is the filter-response function of the linear system. The continuous convolution in (105) is discretized to obtain the linear convolution in a general form

$$H^*(j\Delta) = \sum_{i=-\infty}^{\infty} h(i\Delta) \cdot L^*[(j-i)\Delta] \quad (106)$$

where

$$\Delta = \frac{\ln(10)}{N_{\mathrm{DEC}}} \quad (107)$$

$$L^*(x) = \int_{-\infty}^{\infty} P(\frac{y}{\Delta}) L(x-y) dy = P(\frac{y}{\Delta}) * L(y) \quad (108)$$

$$P(y) = a\frac{\sin(\pi y)}{\sinh(\pi a y)} = \mathrm{sinsh}(y) \quad (109)$$

where $L^*[(j-i)\Delta]$ is the linear digital-filter response, Δ is the sampling interval, N_{DEC} is the number of samples per decade, H^* is the approximation of H, $P(y)$ is the interpolation function, and a is the smoothness parameter. The filter coefficients $L^*(j\Delta)$ may be calculated by using the convolution theorem. H^* is obtained at discrete points as a discrete convolution between the samples of h and $L^*(j\Delta)$. Based on the characteristic of the input function $h(k_\rho)$ and a scheduled truncation tolerance parameter, the sampling interval and the length of digital filter coefficients can be determined. In order to adequately capture the behavior of the input function near the singularities, N_{DEC} is chosen as 350 in this paper. $k_{\rho 1}$ in the deformed integration path is set to be 0.015 k_0 and the number of expansion terms is selected as 27. The smoothness parameter a is set as 8.3764×10^{-3} for the numerical examples.

V. Numerical Examples and Discussions

Various examples will be considered in this section in order to investigate the accuracy and efficiency of the proposed algorithm through the calculation of the dyadic Green's function for the planar multilayered structure depicted in Fig. 3 where the uppermost layer is taken to be free space while the lowermost layer is PEC. The operating frequency is 3 GHz for all examples.

A. Comparison of Numerical Results in the Spectral Domain

In the case of isotropic medium, it is known that the formulation of the correlation between the Green's function in the elec-

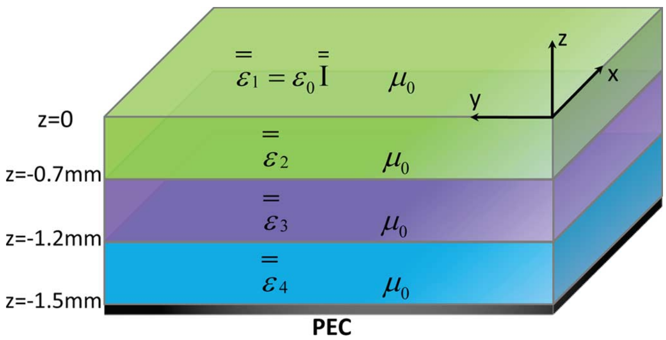

Fig. 3. Geometry of a four-layer medium.

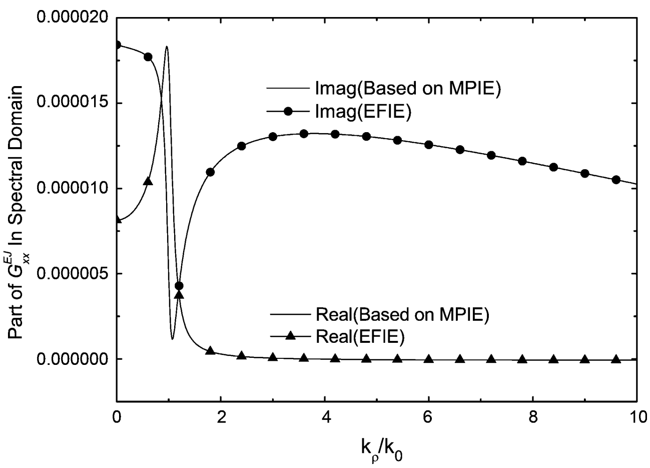

Fig. 4. Magnitude of $\tilde{G}_{xx}^{EJ}$ versus k_ρ for the four-layer isotropic medium with the following parameters: $z' = 0$ mm; $z = -1.2$ mm; layer 2: $\varepsilon_2 = 2.1\varepsilon_0$; layer 3: $\varepsilon_3 = 9.8\varepsilon_0$; layer 4: $\varepsilon_4 = 8.6\varepsilon_0$. The solid lines correspond to results obtained by the presented algorithm while the dots correspond to results from the MPIE.

tric-field integral equation (EFIE) and that in the mixed-potential integral equation (MPIE) is given by

$$\overline{\overline{G}}^{EJ} = i\omega\mu_0\overline{\overline{G}}^{AJ} + \frac{1}{i\omega\varepsilon_0}\nabla\nabla' G^{VJ} \tag{110}$$

where $\overline{\overline{G}}^{AJ}$ represents the dyadic Green's functions for magnetic vector potential and G^{VJ} represents the Green's function for electric scalar potential. It should be noted that the formulations of the dyadic Green's function used in the MPIE have been well documented [31]. Here, one element of the dyadic Green's function obtained by the presented algorithm are compared with the corresponding results from the Green's function used in the MPIE for a four-layer planar isotropic medium, as shown in Fig. 3. Fig. 4 depicts the spectrum of G_{xx}^{EJ} corresponding to Bessel function J_2. It is evident from the resultant plots that the spectral-domain Green's functions obtained by the proposed algorithm agree very well with the existing results from the MPIE when reduced to the isotropic case. The accuracy of the dyadic Green's function in the spectral domain has been validated.

B. Comparison of Numerical Results in the Spatial Domain

The MFHT method is employed for the approximation of the spatial-domain Green's functions for a four-layer planar uniaxial anisotropic medium, as shown in Fig. 3. Fig. 5 depicts the

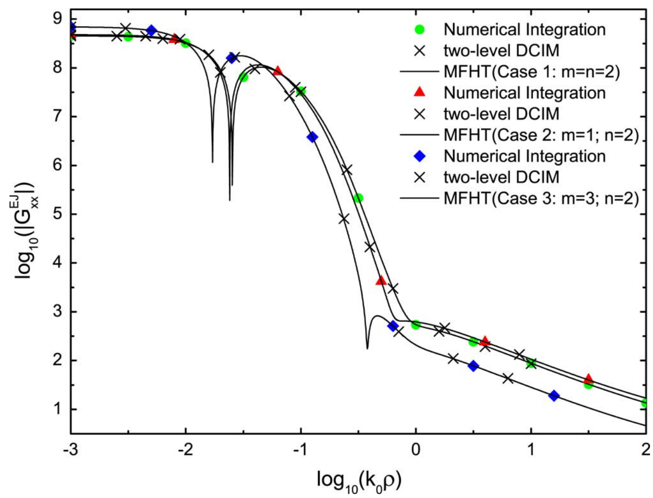

Fig. 5. Magnitudes of G_{xx}^{EJ} versus ρ for the four-layer structure with the following parameters. Case 1: $z' = -0.7$ mm, $z = -0.1$ mm, $\varepsilon_z^{(2,3,4)}/\varepsilon_t^{(2,3,4)} = 1.1$; Case 2: $z' = 0$ mm, $z = -0.7$ mm, $\varepsilon_z^{(2,3,4)}/\varepsilon_t^{(2,3,4)} = 1.5$; Case 3: $z' = -1.2$ mm, $z = -0.6$ mm, $\varepsilon_z^{(2,3,4)}/\varepsilon_t^{(2,3,4)} = 2.0$. The solid lines correspond to results obtained by the MFHT method, while the dots correspond to results obtained by the numerical integration and DCIM.

magnitude of the element G_{xx}^{EJ} of the dyadic Green's function. In the three cases of Fig. 5, the following parameters are kept unchanged: $\varepsilon_t^{(2)} = 2.1\varepsilon_0$, $\varepsilon_t^{(3)} = 9.8\varepsilon_0$, and $\varepsilon_t^{(4)} = 8.6\varepsilon_0$. The parameters that are changed for the three cases are as follows. In the first case, $m = n = 2$, $z' = -0.7$ mm, $z = -0.1$ mm, and $\varepsilon_z^{(2,3,4)}/\varepsilon_t^{(2,3,4)} = 1.1$. In the second case, $m = 1$, $n = 2$, $z' = 0$ mm, $z = -0.7$ mm, and $\varepsilon_z^{(2,3,4)}/\varepsilon_t^{(2,3,4)} = 1.5$. In the third case, $m = 3$, $n = 2$, $z' = -1.2$ mm, $z = -0.6$ mm, and $\varepsilon_z^{(2,3,4)}/\varepsilon_t^{(2,3,4)} = 2.0$. The solid lines represent the results obtained by the MFHT method, while the reference results obtained by numerical integration are represented by the discrete points in the plots. The DCIM-based numerical results are represented by the symbol $\times$. Clearly, the MFHT-based results are in excellent agreement with the numerical integration results and DCIM-based results. The results appear to confirm that based on the MFHT method, the dyadic Green's function for the planar multilayered uniaxial anisotropic medium can be calculated accurately.

Table I shows the computational time for calculating the dyadic Green's function based on the direct numerical integration (DNI), two-level DCIM, and MFHT technique, respectively. We have used the same 2.8-GHz PC to run all these numerical experiments (based on FORTRAN). Compared with the computational time taken by DNI, the time of the MFHT method listed in the fifth line of Table I is very short for calculating the Green's function at one observation point. Fig. 5 shows there is excellent agreement between the results of DNI and that of the MFHT method. From the comparison of accuracy and efficiency between the two methods, it can be deduced that the MFHT method could be an attractive alternative to the rigorous, but computationally expensive DNI technique. The third and fourth lines in Table I show the computational times for the three cases in Fig. 5 based on the two-level DCIM and MFHT method, respectively. It is observed that the

TABLE I
COMPARISON OF THE CPU TIME FOR COMPUTING DYADIC GREEN'S FUNCTION IN SPACE DOMAIN (BASED ON INTEL DUO CORE2 2.8-GHz PC RUNNING FORTRAN)

Example	DNI sec./per point	DCIM sec.	MFHT sec.	MFHT sec./per point
Case 1 in Fig.5	179.02	116.14	46.72	0.875
Case 2 in Fig.5	413.68	122.30	106.89	1.312
Case 3 in Fig.5	413.20	137.13	106.70	1.407
200 Different Cases*	-	≈ 20,000	≈ 300	-

* Without loss of the generality, 200 different numerical experiments are conducted. The vertical position of the observation point is changed for 200 times, while the position of the source point is fixed.

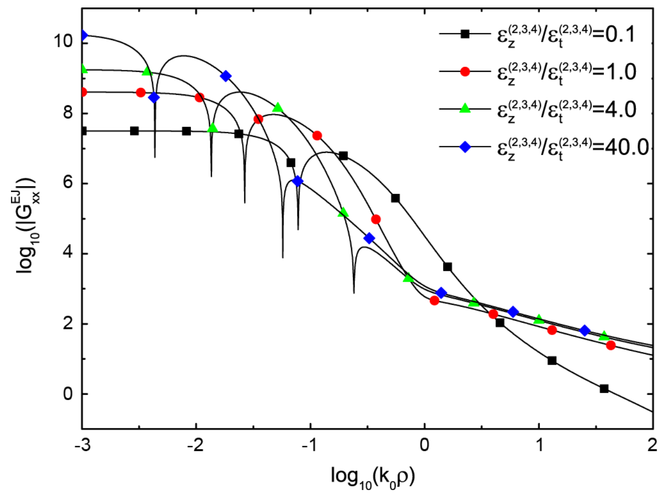

Fig. 6. Magnitudes of G_{xx}^{EJ} versus ρ for the four-layer structure with the following parameters: $m = n = 2$; $z' = -0.7$ mm; $z = -0.1$ mm; layer 2: $\varepsilon_t^{(2)} = 2.1\varepsilon_0$; layer 3: $\varepsilon_t^{(3)} = 9.8\varepsilon_0$; layer 4: $\varepsilon_t^{(4)} = 8.6\varepsilon_0$; $\varepsilon_z^{(2,3,4)}/\varepsilon_t^{(2,3,4)} = 0.1/1.0/4.0/40.0$.

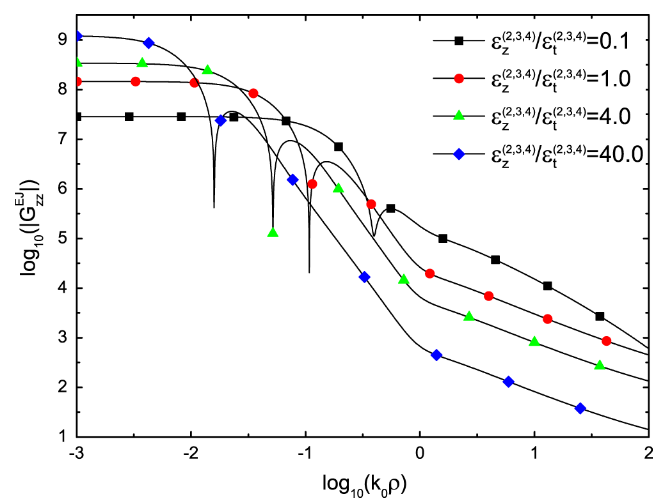

Fig. 7. Magnitudes of G_{zz}^{EJ} versus ρ for the four-layer structure with the following parameters: $m = 1$; $n = 3$; $z' = 0$ mm; $z = -1.2$ mm; layer 2: $\varepsilon_t^{(2)} = 2.1\varepsilon_0$; layer 3: $\varepsilon_t^{(3)} = 9.8\varepsilon_0$; layer 4: $\varepsilon_t^{(4)} = 8.6\varepsilon_0$; $\varepsilon_z^{(2,3,4)}/\varepsilon_t^{(2,3,4)} = 0.1/1.0/4.0/40.0$.

MFHT method requires less time than the DCIM for the three experiments. Here, in order to adequately sample the spectrum of the Green's function, the number of sampling points on each level of the DCIM is 1024. 1024 is one of the best choices for the accuracy of the GPOF technique, which is used in the DCIM method. The maximum relative truncation error of the MFHT method is set to be 10^{-7}, in order to obtain accurate results in a wide field area. With similar accuracy criteria, it seems that the MFHT method performs better than the DCIM in terms of efficiency. Moreover, it is worth mentioning that the forms of the numerical results calculated by the DCIM and MFHT are totally different. The closed-form Green's function is obtained by the DCIM, while the MFHT method is employed to compute the Green's function on discrete points. Table I also lists the computational time for 200 different numerical experiments, based on the two-level DCIM and MFHT method. In 200 experiments, the position of the source point is fixed and the vertical position of the observation point is changed. It is clearly demonstrated that the closed-form Green's function obtained by the DCIM offers no apparent superiority and the computational efficiency of the MFHT method is almost 65 times higher than that of the DCIM. In the practical applications of multilayered medium, such as a microstrip antenna, when the vertical position of the feeding point or field point needs to be changed frequently, the MFHT method can be a powerful tool for the calculation of the multilayered Green's functions.

C. Influence of Material Anisotropy

For the final example considered in this paper, we seek to examine another aspect of the proposed algorithm's accuracy as well as to investigate the influence of material anisotropy on the dyadic Green's function. The accuracy of this algorithm has not been sufficiently validated since the closed-form Green's functions used in the EFIE in the planar multilayered uniaxial anisotropic media have not been derived thus far. However, we can validate the accuracy implicitly through numerical examples. Fig. 6 shows the magnitude of G_{xx}^{EJ} with $z' = -0.7$ mm and $z = -0.1$ mm. Fig. 7 shows the magnitude of G_{zz}^{EJ} with $z' = 0$ mm and $z = -1.2$ mm and Fig. 8 shows the magnitude of G_{xz}^{EJ} with $z' = -1.2$ mm and $z = -0.1$ mm. For the three figures, $\varepsilon_t^{(2)} = 2.1\varepsilon_0$, $\varepsilon_t^{(3)} = 9.8\varepsilon_0$, $\varepsilon_t^{(4)} = 8.6\varepsilon_0$, and $\varepsilon_z^{(2,3,4)}/\varepsilon_t^{(2,3,4)} = 0.1/1.0/4.0/40.0$. Clearly, the closer the value of $\varepsilon_z/\varepsilon_t$ is progressively decreased to 1.0, the closer the magnitudes of the dyadic Green's function are to the results for the case where $\varepsilon_z/\varepsilon_t = 1.0$. It is worth mentioning that the results of the field Green's functions corresponding to $\varepsilon_z/\varepsilon_t = 1.0$ are accurate since the accuracy of the spectral-domain Green's functions reduced to the isotropic case have been validated earlier. This serves as an indication that the presented algorithm for deriving the dyadic Green's function is correct. Figs. 9 and 10 depict the 3-D magnitudes of G_{xx}^{EJ} and G_{xz}^{EJ}, respectively, with $\varepsilon_t^{(2)} = 2.1\varepsilon_0$, $\varepsilon_z^{(2)} = 2\varepsilon_t^{(2)}$, $\varepsilon_t^{(3)} = 9.8\varepsilon_0$, $\left(\varepsilon_z^{(3)} - \varepsilon_t^{(3)}\right)/\varepsilon_0 = -9.0 \sim 9.0$, $\varepsilon_t^{(4)} = 8.6\varepsilon_0$, and $\varepsilon_z^{(4)} = 2\varepsilon_t^{(4)}$. The two plots clearly show the influence of material anisotropy on the Green's functions. It is noted that, as the value of $\left(\varepsilon_z^{(3)} - \varepsilon_t^{(3)}\right)$ increases, the values of the dyadic Green's function increase in the near field and decrease in the intermediate field. This implies that in the multilayered medium, the

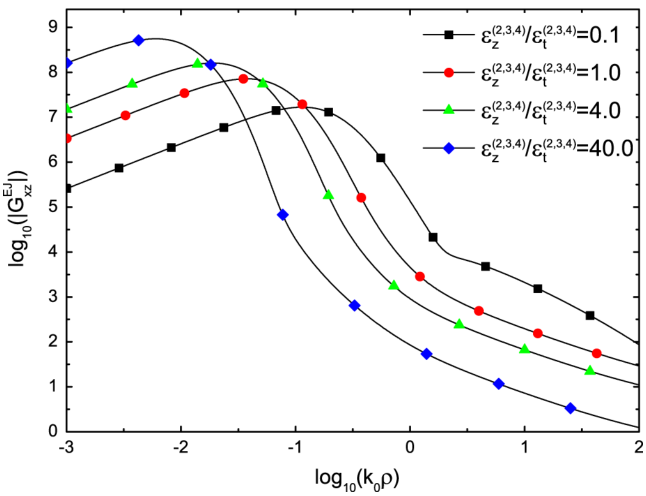

Fig. 8. Magnitudes of G_{xz}^{EJ} versus ρ for the four-layer structure with the following parameters: $m = 3$; $n = 2$; $z' = -1.2$ mm; $z = -0.1$ mm; layer 2: $\varepsilon_t^{(2)} = 2.1\varepsilon_0$; layer 3: $\varepsilon_t^{(3)} = 9.8\varepsilon_0$; layer 4: $\varepsilon_t^{(4)} = 8.6\varepsilon_0$; $\varepsilon_z^{(2,3,4)}/\varepsilon_t^{(2,3,4)} = 0.1/1.0/4.0/40.0$.

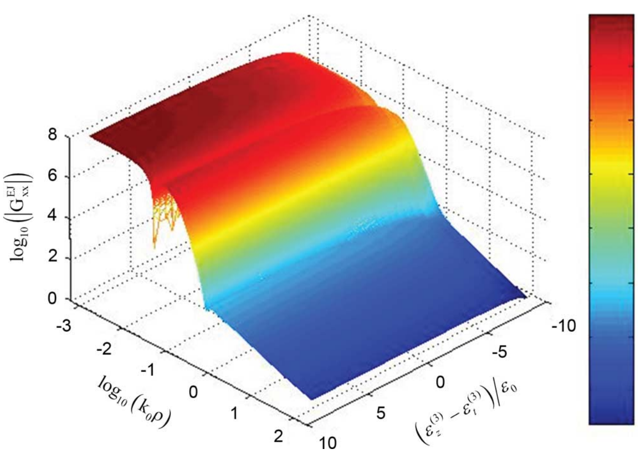

Fig. 9. 3-D magnitudes of G_{xx}^{EJ} versus ρ and permittivity tensor for the four-layer structure with the following parameters: $m = 1$; $n = 3$; $z' = 0$ mm; $z = -1.2$ mm; layer 2: $\varepsilon_t^{(2)} = 2.1\varepsilon_0$, $\varepsilon_z^{(2)} = 2\varepsilon_t^{(2)}$; layer 3: $\varepsilon_t^{(3)} = 9.8\varepsilon_0$, $\left(\varepsilon_z^{(3)} - \varepsilon_t^{(3)}\right)/\varepsilon_0 = -9.0 \sim 9.0$; layer 4: $\varepsilon_t^{(4)} = 8.6\varepsilon_0$, $\varepsilon_z^{(4)} = 2\varepsilon_t^{(4)}$.

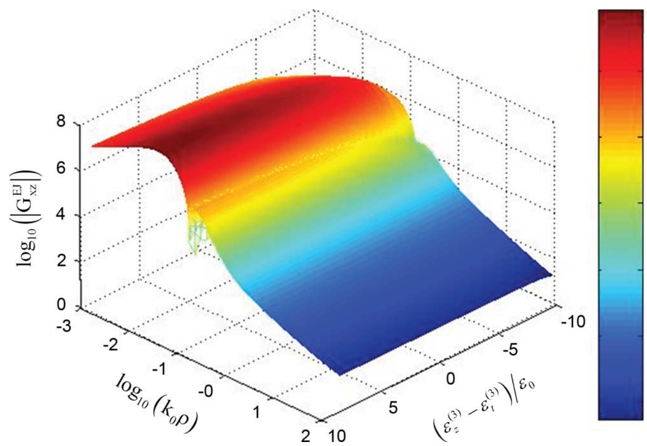

Fig. 10. 3-D magnitudes of G_{xz}^{EJ} versus ρ and permittivity tensor for the four-layer structure with the following parameters: $m = 1$; $n = 3$; $z' = 0$ mm; $z = -1.2$ mm; layer 2: $\varepsilon_t^{(2)} = 2.1\varepsilon_0$, $\varepsilon_z^{(2)} = 2\varepsilon_t^{(2)}$; layer 3: $\varepsilon_t^{(3)} = 9.8\varepsilon_0$, $\left(\varepsilon_z^{(3)} - \varepsilon_t^{(3)}\right)/\varepsilon_0 = -9.0 \sim 9.0$; layer 4: $\varepsilon_t^{(4)} = 8.6\varepsilon_0$, $\varepsilon_z^{(4)} = 2\varepsilon_t^{(4)}$.

value of electric field increases in the near field and decreases in the intermediate field as the material anisotropy increases. The investigation of the material anisotropy's characteristic can pave the way for the practical application of multilayered uniaxial anisotropic media.

VI. Conclusion

In this paper, a systematic and fast algorithm has been presented for the rigorous determination of the dyadic Green's functions in the planar multilayered uniaxial anisotropic media. This algorithm employs the kDB coordinate system to obtain the characteristic field vectors and uses a Fourier transform to derive the unbounded Green's function. One important contribution of the proposed algorithm is that a complete and generalized set of the spectral-domain Green's function in the planar multilayered uniaxial anisotropic media has been derived. Based on the MFHT method, the fast solutions of the spatial-domain Green's function are obtained for the multilayered uniaxial anisotropic media. The MFHT technique has been introduced and its excellent efficiency has been numerically demonstrated. To validate the proposed algorithm and the accuracy of the dyadic Green's function, the numerical examples are implemented in both the spectral domain and spatial domain. The numerical results have been shown to be very accurate and computationally efficient. It paves the path to model emerging microwave and optical devices involving composite birefringent materials.

Appendix

For the case of $m = n$, the dyadic Green's function in the planar multilayered uniaxial anisotropic medium is given by

$$
\begin{aligned}
\overline{\overline{G}}_{nn}(\mathbf{r},\mathbf{r}') &= \frac{1}{i\omega\hat{z}\cdot\overline{\overline{\varepsilon}}_n\cdot\hat{z}}\hat{z}\,\hat{z}\delta(\mathbf{r}-\mathbf{r}') \\
&\quad - \frac{\omega\mu_n}{4\pi}\int_0^\infty dk_\rho\, k_\rho\cdot J_0(k_\rho\rho) \\
&\quad \cdot \Big[e^{ik_{zo}^{(n)}|z_n-z_n'|}\mathbf{e}_{o\beta}^{(n)}\mathbf{u}_{o\beta}^{(n)} + e^{ik_{ze}^{(n)}|z_n-z_n'|}\mathbf{e}_{e\beta}^{(n)}\mathbf{u}_{e\beta}^{(n)} \\
&\qquad + e^{ik_{zo}^{(n)}(z_n-z_n')}A_1^{(1,1)}\mathbf{e}_{ou}^{(n)}\mathbf{u}_{ou}^{(n)} \\
&\qquad + e^{ik_{zo}^{(n)}z_n-ik_{ze}^{(n)}z_n'}A_1^{(1,2)}\mathbf{e}_{ou}^{(n)}\mathbf{u}_{eu}^{(n)} \\
&\qquad + e^{ik_{ze}^{(n)}z_n-ik_{zo}^{(n)}z_n'}A_1^{(2,1)}\mathbf{e}_{eu}^{(n)}\mathbf{u}_{ou}^{(n)} \\
&\qquad + e^{ik_{ze}^{(n)}(z_n-z_n')}A_1^{(2,2)}\mathbf{e}_{eu}^{(n)}\mathbf{u}_{eu}^{(n)} \\
&\qquad + e^{ik_{zo}^{(n)}(z_n+z_n')}A_2^{(1,1)}\mathbf{e}_{ou}^{(n)}\mathbf{u}_{od}^{(n)} \\
&\qquad + e^{ik_{zo}^{(n)}z_n+ik_{ze}^{(n)}z_n'}A_2^{(1,2)}\mathbf{e}_{ou}^{(n)}\mathbf{u}_{ed}^{(n)} \\
&\qquad + e^{ik_{ze}^{(n)}z_n+ik_{zo}^{(n)}z_n'}A_2^{(2,1)}\mathbf{e}_{eu}^{(n)}\mathbf{u}_{od}^{(n)} \\
&\qquad + e^{ik_{ze}^{(n)}(z_n+z_n')}A_2^{(2,2)}\mathbf{e}_{eu}^{(n)}\mathbf{u}_{ed}^{(n)} \\
&\qquad + e^{-ik_{zo}^{(n)}(z_n+z_n')}A_3^{(1,1)}\mathbf{e}_{od}^{(n)}\mathbf{u}_{ou}^{(n)} \\
&\qquad + e^{-ik_{zo}^{(n)}z_n-ik_{ze}^{(n)}z_n'}A_3^{(1,2)}\mathbf{e}_{od}^{(n)}\mathbf{u}_{eu}^{(n)} \\
&\qquad + e^{-ik_{ze}^{(n)}z_n-ik_{zo}^{(n)}z_n'}A_3^{(2,1)}\mathbf{e}_{ed}^{(n)}\mathbf{u}_{ou}^{(n)} \\
&\qquad + e^{-ik_{ze}^{(n)}(z_n+z_n')}A_3^{(2,2)}\mathbf{e}_{ed}^{(n)}\mathbf{u}_{eu}^{(n)} \\
&\qquad + e^{-ik_{zo}^{(n)}(z_n-z_n')}A_4^{(1,1)}\mathbf{e}_{od}^{(n)}\mathbf{u}_{od}^{(n)}
\end{aligned}
$$

$$\begin{aligned}&+e^{-ik_{zo}^{(n)}z_n+ik_{ze}^{(n)}z'_n}A_4^{(1,2)}\mathbf{e}_{od}^{(n)}\mathbf{u}_{ed}^{(n)}\\&+e^{-ik_{ze}^{(n)}z_n+ik_{zo}^{(n)}z'_n}A_4^{(2,1)}\mathbf{e}_{ed}^{(n)}\mathbf{u}_{od}^{(n)}\\&+e^{-ik_{ze}^{(n)}(z_n-z'_n)}A_4^{(2,2)}\mathbf{e}_{ed}^{(n)}\mathbf{u}_{ed}^{(n)}\Big]\end{aligned}\tag{111}$$

where

$$\mathbf{A}_2=[\mathbf{G}_u^{(n)}(z_n=-D_n)]^{-1}\cdot\mathbf{R}_{Dn}\cdot\mathbf{N}_n\cdot\mathbf{G}_d^{(n)}(z_n=-D_n)\tag{112}$$

$$\mathbf{A}_1=\mathbf{A}_2\cdot\mathbf{G}_d^{(n)}(z_n=D_{n-1})\cdot\mathbf{R}_{Un}\cdot\mathbf{G}_u^{(n)}(z_n=-D_{n-1})\tag{113}$$

$$\begin{aligned}\mathbf{A}_3=&[\mathbf{G}_d^{(n)}(z_n=-D_{n-1})]^{-1}\cdot\mathbf{R}_{Un}\cdot\mathbf{M}_n\\&\cdot\mathbf{G}_u^{(n)}(z_n=-D_{n-1})\end{aligned}\tag{114}$$

$$\mathbf{A}_4=\mathbf{A}_3\cdot\mathbf{G}_u^{(n)}(z_n=D_n)\cdot\mathbf{R}_{Dn}\cdot\mathbf{G}_d^{(n)}(z_n=-D_n)\tag{115}$$

$$\begin{aligned}\mathbf{M}_n=&[\mathbf{I}-\mathbf{G}_u^{(n)}(z_n=-D_{n-1}+D_n)\cdot\mathbf{R}_{Dn}\\&\cdot\mathbf{G}_d^{(n)}(z_n=-D_n+D_{n-1})\cdot\mathbf{R}_{Un}]^{-1}\end{aligned}\tag{116}$$

$$\begin{aligned}\mathbf{N}_n=&[\mathbf{I}-\mathbf{G}_d^{(n)}(z_n=-D_n+D_{n-1})\cdot\mathbf{R}_{Un}\\&\cdot\mathbf{G}_u^{(n)}(z_n=-D_{n-1}+D_n)\cdot\mathbf{R}_{Dn}]^{-1}\end{aligned}\tag{117}$$

J_0 is the Bessel function of zeroth order. When the source point z' is located above the observation point z, β in (111) is equal to d. Otherwise, β is equal to u.

From (92), it is easy to obtain an explicit expression for the dyadic Green's function $\mathbf{G}_{nm}(\mathbf{r},\mathbf{r}')$ for the case of $m>n$. This yields

$$\begin{aligned}&\overline{\overline{G}}_{nm}(\mathbf{r},\mathbf{r}')\\&=-\frac{\omega\mu_m}{4\pi}\int_0^\infty dk_\rho\,k_\rho\cdot J_0(k_\rho\rho)\\&\cdot\Big[e^{ik_{zo}^{(n)}(z_n+D_n)-ik_{zo}^{(m)}(z'_m+D_{m-1})}B_1^{(1,1)}\mathbf{e}_{ou}^{(n)}\mathbf{u}_{ou}^{(m)}\\&+e^{ik_{zo}^{(n)}(z_n+D_n)-ik_{ze}^{(m)}(z'_m+D_{m-1})}B_1^{(1,2)}\mathbf{e}_{ou}^{(n)}\mathbf{u}_{eu}^{(m)}\\&+e^{ik_{ze}^{(n)}(z_n+D_n)-ik_{zo}^{(m)}(z'_m+D_{m-1})}B_1^{(2,1)}\mathbf{e}_{eu}^{(n)}\mathbf{u}_{ou}^{(m)}\\&+e^{ik_{ze}^{(n)}(z_n+D_n)-ik_{ze}^{(m)}(z'_m+D_{m-1})}B_1^{(2,2)}\mathbf{e}_{eu}^{(n)}\mathbf{u}_{eu}^{(m)}\\&+e^{ik_{zo}^{(n)}(z_n+D_n)+ik_{zo}^{(m)}(z'_m+D_m)}B_2^{(1,1)}\mathbf{e}_{ou}^{(n)}\mathbf{u}_{od}^{(m)}\\&+e^{ik_{zo}^{(n)}(z_n+D_n)+ik_{ze}^{(m)}(z'_m+D_m)}B_2^{(1,2)}\mathbf{e}_{ou}^{(n)}\mathbf{u}_{ed}^{(m)}\\&+e^{ik_{ze}^{(n)}(z_n+D_n)+ik_{zo}^{(m)}(z'_m+D_m)}B_2^{(2,1)}\mathbf{e}_{eu}^{(n)}\mathbf{u}_{od}^{(m)}\\&+e^{ik_{ze}^{(n)}(z_n+D_n)+ik_{ze}^{(m)}(z'_m+D_m)}B_2^{(2,2)}\mathbf{e}_{eu}^{(n)}\mathbf{u}_{ed}^{(m)}\\&+e^{-ik_{zo}^{(n)}(z_n+D_{n+1})-ik_{zo}^{(m)}(z'_m+D_{m-1})}B_3^{(1,1)}\mathbf{e}_{od}^{(n)}\mathbf{u}_{ou}^{(m)}\\&+e^{-ik_{zo}^{(n)}(z_n+D_{n+1})-ik_{ze}^{(m)}(z'_m+D_{m-1})}B_3^{(1,2)}\mathbf{e}_{od}^{(n)}\mathbf{u}_{eu}^{(m)}\\&+e^{-ik_{ze}^{(n)}(z_n+D_{n+1})-ik_{zo}^{(m)}(z'_m+D_{m-1})}B_3^{(2,1)}\mathbf{e}_{ed}^{(n)}\mathbf{u}_{ou}^{(m)}\\&+e^{-ik_{ze}^{(n)}(z_n+D_{n+1})-ik_{ze}^{(m)}(z'_m+D_{m-1})}B_3^{(2,2)}\mathbf{e}_{ed}^{(n)}\mathbf{u}_{eu}^{(m)}\\&+e^{-ik_{zo}^{(n)}(z_n+D_{n+1})+ik_{zo}^{(m)}(z'_m+D_m)}B_4^{(1,1)}\mathbf{e}_{od}^{(n)}\mathbf{u}_{od}^{(m)}\\&+e^{-ik_{zo}^{(n)}(z_n+D_{n+1})+ik_{ze}^{(m)}(z'_m+D_m)}B_4^{(1,2)}\mathbf{e}_{od}^{(n)}\mathbf{u}_{ed}^{(m)}\\&+e^{-ik_{ze}^{(n)}(z_n+D_{n+1})+ik_{zo}^{(m)}(z'_m+D_m)}B_4^{(2,1)}\mathbf{e}_{ed}^{(n)}\mathbf{u}_{od}^{(m)}\\&+e^{-ik_{ze}^{(n)}(z_n+D_{n+1})+ik_{ze}^{(m)}(z'_m+D_m)}B_4^{(2,2)}\mathbf{e}_{ed}^{(n)}\mathbf{u}_{ed}^{(m)}\Big]\end{aligned}\tag{118}$$

where

$$\mathbf{B}_1=\mathbf{Y}_{mn}^{(u)}\cdot\mathbf{M}_m\tag{119}$$

$$\mathbf{B}_2=\mathbf{B}_1\cdot\mathbf{G}_u^{(m)}(z_m=-D_{m-1}+D_m)\cdot\mathbf{R}_{Dm}\tag{120}$$

$$\mathbf{B}_3=\mathbf{R}_{Un}\cdot\mathbf{G}_u^{(n)}(z_n=-D_{n-1}+D_n)\cdot\mathbf{B}_1\tag{121}$$

$$\mathbf{B}_4=\mathbf{B}_3\cdot\mathbf{G}_u^{(m)}(z_m=-D_{m-1}+D_m)\cdot\mathbf{R}_{Dm}.\tag{122}$$

Similarly, the explicit expression of the dyadic Green's function for the case of $m<n$ is given by

$$\begin{aligned}&\overline{\overline{G}}_{nm}(\mathbf{r},\mathbf{r}')\\&=-\frac{\omega\mu_m}{4\pi}\int_0^\infty dk_\rho\,k_\rho\cdot J_0(k_\rho\rho)\\&\cdot\Big[e^{ik_{zo}^{(n)}(z_n+D_n)-ik_{zo}^{(m)}(z'_m+D_{m-1})}C_1^{(1,1)}\mathbf{e}_{ou}^{(n)}\mathbf{u}_{ou}^{(m)}\\&+e^{ik_{zo}^{(n)}(z_n+D_n)-ik_{ze}^{(m)}(z'_m+D_{m-1})}C_1^{(1,2)}\mathbf{e}_{ou}^{(n)}\mathbf{u}_{eu}^{(m)}\\&+e^{ik_{ze}^{(n)}(z_n+D_n)-ik_{zo}^{(m)}(z'_m+D_{m-1})}C_1^{(2,1)}\mathbf{e}_{eu}^{(n)}\mathbf{u}_{ou}^{(m)}\\&+e^{ik_{ze}^{(n)}(z_n+D_n)-ik_{ze}^{(m)}(z'_m+D_{m-1})}C_1^{(2,2)}\mathbf{e}_{eu}^{(n)}\mathbf{u}_{eu}^{(m)}\\&+e^{ik_{zo}^{(n)}(z_n+D_n)+ik_{zo}^{(m)}(z'_m+D_m)}C_2^{(1,1)}\mathbf{e}_{ou}^{(n)}\mathbf{u}_{od}^{(m)}\\&+e^{ik_{zo}^{(n)}(z_n+D_n)+ik_{ze}^{(m)}(z'_m+D_m)}C_2^{(1,2)}\mathbf{e}_{ou}^{(n)}\mathbf{u}_{ed}^{(m)}\\&+e^{ik_{ze}^{(n)}(z_n+D_n)+ik_{zo}^{(m)}(z'_m+D_m)}C_2^{(2,1)}\mathbf{e}_{eu}^{(n)}\mathbf{u}_{od}^{(m)}\\&+e^{ik_{ze}^{(n)}(z_n+D_n)+ik_{ze}^{(m)}(z'_m+D_m)}C_2^{(2,2)}\mathbf{e}_{eu}^{(n)}\mathbf{u}_{ed}^{(m)}\\&+e^{-ik_{zo}^{(n)}(z_n+D_{n-1})-ik_{zo}^{(m)}(z'_m+D_{m-1})}C_3^{(1,1)}\mathbf{e}_{od}^{(n)}\mathbf{u}_{ou}^{(m)}\\&+e^{-ik_{zo}^{(n)}(z_n+D_{n-1})-ik_{ze}^{(m)}(z'_m+D_{m-1})}C_3^{(1,2)}\mathbf{e}_{od}^{(n)}\mathbf{u}_{eu}^{(m)}\\&+e^{-ik_{ze}^{(n)}(z_n+D_{n-1})-ik_{zo}^{(m)}(z'_m+D_{m-1})}C_3^{(2,1)}\mathbf{e}_{ed}^{(n)}\mathbf{u}_{ou}^{(m)}\\&+e^{-ik_{ze}^{(n)}(z_n+D_{n-1})-ik_{ze}^{(m)}(z'_m+D_{m-1})}C_3^{(2,2)}\mathbf{e}_{ed}^{(n)}\mathbf{u}_{eu}^{(m)}\\&+e^{-ik_{zo}^{(n)}(z_n+D_{n-1})+ik_{zo}^{(m)}(z'_m+D_m)}C_4^{(1,1)}\mathbf{e}_{od}^{(n)}\mathbf{u}_{od}^{(m)}\\&+e^{-ik_{zo}^{(n)}(z_n+D_{n-1})+ik_{ze}^{(m)}(z'_m+D_m)}C_4^{(1,2)}\mathbf{e}_{od}^{(n)}\mathbf{u}_{ed}^{(m)}\\&+e^{-ik_{ze}^{(n)}(z_n+D_{n-1})+ik_{zo}^{(m)}(z'_m+D_m)}C_4^{(2,1)}\mathbf{e}_{ed}^{(n)}\mathbf{u}_{od}^{(m)}\\&+e^{-ik_{ze}^{(n)}(z_n+D_{n-1})+ik_{ze}^{(m)}(z'_m+D_m)}C_4^{(2,2)}\mathbf{e}_{ed}^{(n)}\mathbf{u}_{ed}^{(m)}\Big]\end{aligned}\tag{123}$$

where

$$\mathbf{C}_4=\mathbf{Y}_{mn}^{(d)}\cdot\mathbf{N}_m\tag{124}$$

$$\mathbf{C}_3=\mathbf{C}_4\cdot\mathbf{G}_d^{(m)}(z_m=-D_m+D_{m-1})\cdot\mathbf{R}_{Dm}\tag{125}$$

$$\mathbf{C}_2=\mathbf{R}_{Dn}\cdot\mathbf{G}_d^{(n)}(z_n=-D_n+D_{n-1})\cdot\mathbf{C}_4\tag{126}$$

$$\mathbf{C}_1=\mathbf{C}_2\cdot\mathbf{G}_d^{(m)}(z_m=-D_m+D_{m-1})\cdot\mathbf{R}_{Um}.\tag{127}$$

REFERENCES

[1] J. R. Mosig, "Arbitrarily shaped microstrip structures and their analysis with a mixed potential integral equation," *IEEE Trans. Microw. Theory Tech.*, vol. 36, no. 2, pp. 314–323, Feb. 1988.

[2] M. J. Tsai, F. D. Flavis, O. Fordharn, and N. G. Alexopoulos, "Modeling planar arbitrarily shaped microstrip elements in multilayered media," *IEEE Trans. Microw. Theory Tech.*, vol. 45, no. 3, pp. 330–337, Mar. 1997.

[3] F. Ling, J. Liu, and J. M. Jin, "Efficient electromagnetic modeling of 3-D multilayer microstrip antennas and circuits," *IEEE Trans. Microw. Theory Tech.*, vol. 50, no. 6, pp. 1628–1635, Jun. 2002.

[4] W. H. Tang and S. D. Gedney, "An efficient application of the discrete complex image method for quasi-3-D microwave circuits in layered media," *IEEE Trans. Microw. Theory Tech.*, vol. 55, no. 8, pp. 1723–1729, Aug. 2007.

[5] D. C. Fang, J. J. Yang, and G. Y. Desisle, "Discrete image theory for horizontal electric dipoles in a multilayered medium," *Proc. IEEE*, vol. 135, no. 5, pp. 297–303, May 1988.

[6] K. A. Michalski and D. Zheng, "Electromagnetic scattering and radiation by surface of arbitrary shape in layered media—Part I: Theory," *IEEE Trans. Antennas Propag.*, vol. 38, no. 3, pp. 335–344, Mar. 1990.

[7] Y. L. Chow, J. J. Yang, D. G. Fang, and G. E. Howard, "A closed-form spatial Green's function for the thick microstrip substrate," *IEEE Trans. Microw. Theory Tech.*, vol. 39, no. 3, pp. 588–592, Mar. 1991.

[8] W. C. Chew, *Wave and Fields in Inhomogeneous Media*. Piscataway, NJ: IEEE Press, 1995.

[9] G. Dural and M. I. Aksun, "Closed-form Green's functions for general sources and stratified media," *IEEE Trans. Microw. Theory Tech.*, vol. 43, no. 7, pp. 1545–1552, Jul. 1995.

[10] M. I. Aksun, "A robust approach for the derivation of closed-form Green's functions," *IEEE Trans. Microw. Theory Tech.*, vol. 44, no. 5, pp. 651–658, May 1996.

[11] A. C. Cangellaris and V. I. Okhmatovski, "Novel closed-form Green's function in shield planar layered media," *IEEE Trans. Microw. Theory Tech.*, vol. 48, no. 12, pp. 2225–2232, Dec. 2000.

[12] V. I. Okhmatovski and A. C. Cangellaris, "A new technique for the derivation of closed-form electromagnetic Green's functions for unbounded planar layered media," *IEEE Trans. Microw. Theory Tech.*, vol. 50, no. 7, pp. 1005–1016, Jul. 2002.

[13] V. N. Kourkoulos and A. C. Cangellaris, "Accurate approximation of Green's functions in planar stratified media in terms of a finite sum of spherical and cylindrical waves," *IEEE Trans. Antennas Propag.*, vol. 54, no. 5, pp. 1568–1576, May 2006.

[14] C. M. Krowne, "Determination of the Green's function in the spectral domain using a matrix method: Application of radiators or resonators immersed in a complex anisotropic layered medium," *IEEE Trans. Antennas Propag.*, vol. 34, no. 2, pp. 247–253, Feb. 1986.

[15] J. L. Tsalamengas, "Interaction of electromagnetic waves with general bianisotropic slabs," *IEEE Trans. Microw. Theory Tech.*, vol. 40, no. 10, pp. 1870–1878, Oct. 1992.

[16] F. Olyslager and D. D. Zutter, "Rigorous full-wave analysis of electric and dielectric waveguides embedded in a multilayered bianisotropic medium," *Radio Sci.*, vol. 28, no. 5, pp. 937–946, Sep. 1993.

[17] L. W. Li, J. H. Koh, T. S. Yeo, and M. S. Leong, "Analysis of radiowave propagation in a four-layered anisotropic forest environment," *IEEE Trans. Geosci. Remote Sens.*, vol. 37, no. 7, pp. 1967–1979, Jul. 1999.

[18] C. T. Tai, *Dyadic Green Functions in Electromagnetic Theory*. New York: IEEE Press, 1993.

[19] S. M. Ali and S. F. Mahmoud, "Electromagnetic fields of buried sources in stratified anisotropic media," *IEEE Trans. Antennas Propag.*, vol. AP-27, no. 9, pp. 671–678, Sep. 1979.

[20] K. A. Michalski, "Formulation of mixed-potential integral equations for arbitrarily shaped microstrip structures with uniaxial substrates," *J. Electromagn. Waves Appl.*, vol. 7, no. 7, pp. 899–917, 1993.

[21] L.-W. Li, J.-H. Koh, T.-S. Yeo, M.-S. Leong, and P.-S. Kooi, "Cylindrical vector eigenfunction expansion of Green dyadics for multilayered anisotropic media and its application to four-layered forest," *IEEE Trans. Antennas Propag.*, vol. 52, no. 2, pp. 466–477, Feb. 2004.

[22] J. K. Lee and J. A. Kong, "Dyadic Green's functions for layered anisotropic medium," *Electromagn.*, vol. 3, pp. 110–130, Apr. 1983.

[23] T. M. Habashy, S. M. Ali, J. A. Kong, and M. D. Grossi, "Dyadic Green's functions in a planar stratified, arbitrarily magnetized linear plasma," *Radio Sci.*, vol. 26, no. 3, pp. 701–715, May/Jun. 1991.

[24] W. Ren, "Dyadic Green's functions and dipole radiations in layered chiral media," *J. Appl. Phys.*, vol. 75, no. 1, pp. 30–35, Jan. 1994.

[25] C. W. Qiu, S. Zouhdi, and A. Razek, "Modified spherical wave functions with anisotropy ratio: Application of the analysis of scattering by multilayered anisotropic shells," *IEEE Trans. Antennas Propag.*, vol. 55, no. 12, pp. 3515–3523, Dec. 2007.

[26] R. C. Hsieh and J. T. Ku, "Fast full-wave analysis of planar microstrip circuit elements in stratified media," *IEEE Trans. Microw. Theory Tech.*, vol. 46, no. 9, pp. 1291–1297, Sep. 1998.

[27] P. P. Ding, S. Zouhdi, L. W. Li, S. P. Yeo, and N. B. Christensen, "A modified fast Hankel transform algorithm for calculating planar multilayered Green's function," in *Int. Electromagn. Adv. Appl. Conf.*, Sep. 2010, pp. 47–50.

[28] J. A. Kong, *Electromagnetic Wave Theory*. New York: Wiley, 1986.

[29] M. Abramowitz and I. A. Stegun, *Handbook of Mathematical Function*. New York: Dover, 1972.

[30] N. B. Christensen, "Optimized fast Hankel transform filters," *Geophys. Prospecting*, vol. 38, pp. 545–568, Jul. 1990.

[31] M. Zhang, L. W. Li, and Y. F. Tian, "An efficient approach for extracting poles of Green's functions in general multilayered media," *IEEE Trans. Antennas Propag.*, vol. 56, no. 1, pp. 269–273, Jan. 2008.

Ping-Ping Ding, photograph and biography not available at time of publication.

Cheng-Wei Qiu, photograph and biography not available at time of publication.

Saïd Zouhdi (M'99–SM'05), photograph and biography not available at time of publication.

Swee Ping Yeo, photograph and biography not available at time of publication.